Computer Methods in Applied Mechanics and Engineering 455 (2026) 118868

Contents lists available at ScienceDirect

Comput. Methods Appl. Mech. Engrg.

journal homepage: www.elsevier.com/locate/cma

A mixed displacement-pressure-stress stabilized finite element formulation for a finite strain damage model

Inocencio Castañar [a], Ramon Codina [b,c,*], Joan Baiges [b,c]

[a] Department of Mechanical Engineering, Universitat Politècnica de Catalunya–BarcelonaTech (UPC), Escola d'Enginyeria de Barcelona Est, Av. Eduard Maristany 16 Edifici A, 08019, Barcelona, Spain
[b] Department of Civil and Environmental Engineering, Universitat Politècnica de Catalunya–BarcelonaTech (UPC), Jordi Girona 1-3 Edifici C1, 08034, Barcelona, Spain
[c] Centre Internacional de Mètodes Numèrics en Enginyeria, Gran Capità S/N, 08034, Barcelona, Spain

ARTICLE INFO

Keywords:
Mixed three-field formulation
Finite strain
Continuum damage mechanics
Stress accuracy
Stabilization

ABSTRACT

In this work, we describe a finite element formulation for the approximation of solid mechanics problems using a damage model under finite strain conditions. The balance equations are written in a total Lagrangian framework, employing the deviatoric component of the second Piola–Kirchhoff stress tensor, the displacement, and the pressure as primary variables. Introducing the pressure as a variable enables the treatment of incompressible materials, while incorporating the stress improves the stress approximation, which is crucial when nonlinear material laws depending on stress (or strain) are considered. In particular, we adopt the damage model proposed by Comellas et al. (International Journal for Numerical Methods in Engineering, Vol. 105, pp. 781–800, 2016), which generalizes previous isotropic damage models from infinitesimal strains to finite ones. This damage model is combined with a hyperelastic formulation for the reversible component of the deformation.

The three-field formulation we consider was first introduced and analyzed for the Stokes problem by Codina (SIAM Journal on Numerical Analysis, Vol. 47, pp. 699–718, 2009). The interest of interpolating stress as an independent variable was highlighted in the work of Cervera et al. (Computer Methods in Applied Mechanics and Engineering, Vol. 199, pp. 2559–2570, 2010), and has since been successfully applied to numerous problems involving both linear and nonlinear constitutive behavior under the small strain assumption. More recently, Codina et al. (International Journal for Numerical Methods in Engineering, Vol. 125, e7540, 2024), extended the three-field formulation to geometrically nonlinear problems. The purpose of the present work is to combine these approaches, addressing problems that involve both nonlinear constitutive laws and geometrical nonlinearity with a mixed, three-field approach.

1. Introduction

Damage models are among the simplest formulations for capturing the nonlinear behavior of solids associated with localized irreversible deformations and fracture. The fundamental idea is to degrade the elastic stiffness by means of a factor that monotonically increases during the deformation process. These theories are now well established, both experimentally and from a thermodynamical standpoint (see, e.g., [1–5]).

* Corresponding author.
E-mail addresses: inocencio.castanar@upc.edu (I. Castañar), ramon.codina@upc.edu (R. Codina), joan.baiges@upc.edu (J. Baiges).

https://doi.org/10.1016/j.cma.2026.118868

Available online 11 March 2026

Early formulations were developed for infinitesimal strains under the assumption of isotropy, and were later generalized to anisotropic materials [6,7] and to finite strain problems, which is the framework of interest in this work. One of the first contributions to finite strain damage was [8]. Further developments can be found in [9–11], where the starting point is usually the multiplicative decomposition of the deformation gradient into isochoric and volumetric components. In contrast, in this work we adopt the approach proposed in [12], which is based on splitting the hyperelastic energy functional into isochoric and volumetric contributions and introducing a damage law only for the former, thus limiting the possibility to model localization and incompressibility at the same time, as discussed later. In that reference, a generalized softening finite strain model is proposed, incorporating linear and exponential damage evolution laws that extend those used in the infinitesimal strain case. Although this framework allows for large deformations, we do not consider the possibility of buckling.

Once the constitutive model has been selected, the next question concerns the choice of unknowns. In an irreducible setting, the problem can be expressed solely in terms of displacements, with all other variables recovered from them. However, this approach cannot adequately handle incompressible materials, for which pressure must be introduced as an additional variable (see, e.g., [13,14] and references therein). Another key consideration is whether to also include the isochoric stress as an independent variable. This is the strategy adopted here. The main motivation is that it leads to more accurate stress computations while remaining computationally competitive with irreducible formulations, even though it introduces more degrees of freedom per mesh. As shown in [15], mixed formulations allow the use of coarser meshes while achieving comparable accuracy. Although it is not the main focus of this paper, there is a second motivation for including stresses as unknowns: in constitutive models such as damage and plasticity, the material response often depends explicitly on stresses (or strains). Ensuring pointwise convergence of these stresses is essential for mesh-independent results in localization problems [16], which cannot be guaranteed in irreducible formulations unless displacements are sufficiently smooth–a condition rarely satisfied in practical geometries. Using stresses as variables enables such convergence and mesh-independent outcomes, a fact already highlighted in [17,18]. The inclusion of incompressible constitutive laws in this context was addressed in [19]. This purely numerical strategy for handling localization should be regarded as an alternative to regularization techniques such as nonlocal/gradient-enhanced formulations [20,21], phase-field variational fracture models [22,23], and viscoplastic regularization [24]. All these approaches introduce an internal length scale to ensure mesh-objective finite element predictions. While the introduction of stresses as unknowns may also lead to mesh-objective approximations, a detailed study of this phenomenon in finite strain problems lies outside the scope of this paper.

With displacements, deviatoric stresses, and pressure chosen as unknowns, two strategies are available for their finite element (FE) approximation. The first is to design interpolation spaces that satisfy the inf-sup conditions inherited from the continuous problem. However, this typically leads to complex interpolation schemes, especially for stresses. The alternative, which we adopt here, is to employ a stabilized FE formulation based on the Variational MultiScale (VMS) concept [25,26], which allows the use of arbitrary interpolations. In practice, this makes it possible to apply continuous equal-order interpolation for all unknowns. This approach was originally proposed and analyzed for the Stokes problem in [27], and details of its extension to hyperelasticity can be found in [13,14]. In this paper, we focus on its application to damage models.

It is worth noting that alternative mixed interpolations for finite strain damage models can be found in the literature. For example, [28,29] proposed gradient-regularized models to achieve mesh-independent solutions, with different sets of auxiliary variables, while [30] used displacements and the damage variable. Irreducible formulations have also been employed, for instance in [31]. In contrast, our approach uses displacements, pressure, and isochoric stresses as primary unknowns.

The structure of the paper is as follows. In Section 2, we describe the problem to be solved at the continuous level, including the geometry description for finite strains, the damage model in some detail, and the variational formulation of the boundary value problem to be solved, restricted here to the quasi-static case. The numerical approximation is presented in Section 3, starting with the linearization of the continuous equations and stating the stabilized FE formulation we use. Numerical examples are provided in Section 4, and conclusions are drawn in Section 5.

2. Problem statement

2.1. Geometry description

Let $\Omega_0 \subset \mathbb{R}^{\mathrm{d}}$ be the open domain occupied by the solid to be analyzed at a reference configuration, with $\mathrm{d} = 2, 3$, and let Ω be the domain the solid occupies at the deformed configuration. We will be interested in quasi-static processes, so that the way Ω_0 is mapped to Ω along time is irrelevant. The material coordinates in Ω_0 are labelled as $\boldsymbol{X}$. Let $\boldsymbol{x} = \boldsymbol{\psi}(\boldsymbol{X})$ be the mapping from Ω_0 to Ω. The boundary of Ω_0 is denoted by $\Gamma_0 = \partial\Omega_0$.

The gradient deformation tensor $\boldsymbol{F}$ is defined as $\boldsymbol{F} = \frac{\partial \boldsymbol{x}}{\partial \boldsymbol{X}}$, and its determinant as $J = \det(\boldsymbol{F})$. We indicate as $\{\boldsymbol{E}_A\}_{A=1}^{\mathrm{d}}$ the basis vectors at the reference configuration, and $\{\boldsymbol{e}_a\}_{a=1}^{\mathrm{d}}$ the basis vectors at the deformed configuration. In spite of using Cartesian coordinates, this distinction allows one to distinguish to which bases correspond the components of a tensor. In particular, we may write

$$\boldsymbol{F} = F_{aA}\boldsymbol{e}_a \otimes \boldsymbol{E}_A = \frac{\partial x_a}{\partial X_A}\boldsymbol{e}_a \otimes \boldsymbol{E}_A.$$

Einstein summation convention is used here and in what follows, with repeated indexes summing from 1 to d. Lower case Latin letters $a, b, c, \ldots$ will be used for indexes of tensors in the deformed configuration Ω, and upper case Latin letters $A, B, C, \ldots$ for indexes

in the reference configuration Ω_0. We shall also make use of the right Cauchy-Green tensor $\boldsymbol{C}$, defined by

$$C_{AB} = F_{aB}F_{aA}, \tag{1}$$

or, in intrinsic form, $\boldsymbol{C} = \boldsymbol{F}^T \cdot \boldsymbol{F}$.

2.2. Balance equations

The equation for the conservation of mass reads:

$$\rho J = \rho_0, \tag{2}$$

where $\rho = \rho(\boldsymbol{X})$ is the density in the deformed configuration and $\rho_0 = \rho_0(\boldsymbol{X})$ is the density in the reference configuration.

Let $\boldsymbol{\sigma} = \sigma_{ab}\boldsymbol{e}_a \otimes \boldsymbol{e}_b$ be the Cauchy stress tensor, $\boldsymbol{u} = u_a\boldsymbol{e}_a$ the displacement field and $\boldsymbol{f} = f_a\boldsymbol{e}_a$ the vector of external accelerations, all these fields expressed in terms of $\boldsymbol{X}$ but referred to the deformed configuration. Abusing of the notation, we shall use the same symbols when writing them in terms of $\boldsymbol{x}$. Let also $\boldsymbol{S} = S_{AB}\boldsymbol{E}_A \otimes \boldsymbol{E}_B$ be the second Piola-Kirchhoff (PK2) stress tensor, related to $\boldsymbol{\sigma}$ by

$$S_{AB} = J F^{-1}_{Aa} F^{-1}_{Bb} \sigma_{ab}, \tag{3}$$

i.e., $\boldsymbol{S} = J\boldsymbol{F}^{-1} \cdot \boldsymbol{\sigma} \cdot \boldsymbol{F}^{-T}$ in intrinsic form. Note that $\boldsymbol{S}$ is a symmetric tensor.

The conservation of linear momentum can be expressed as

$$-\partial_A(F_{aB}S_{BA}) = \rho_0 f_a, \tag{4}$$

or, in intrinsic form $-\nabla_{\boldsymbol{X}} \cdot (\boldsymbol{S} \cdot \boldsymbol{F}^T) = \rho_0 \boldsymbol{f}$. The notation that we have used is as follows: ∂_A is the partial derivative with respect to X_A and $\nabla_{\boldsymbol{X}}$ is the operator ∇ expressed in the coordinates $\boldsymbol{X}$, so that $\nabla_{\boldsymbol{X}}\cdot$ is the divergence of a vector field expressed in the coordinates $\boldsymbol{X}$.

In the case of exactly incompressible materials, it is necessary to introduce the pressure p as a variable, defined as minus the mean Cauchy stress, so that the Cauchy stress tensor can be split into volumetric and deviatoric components as

$$\sigma_{ab} = -p\delta_{ab} + \sigma^{\text{dev}}_{ab}, \tag{5}$$

where δ_{ab} is the Kronecker symbol, i.e., $\boldsymbol{\sigma} = -p\boldsymbol{I} + \boldsymbol{\sigma}^{\text{dev}}$. With this convention, positive values of p correspond to compressive volumetric states, while tensile volumetric states are associated with negative pressure. This induces the following splitting of tensor $\boldsymbol{S}$:

$$S_{AB} = J F^{-1}_{Aa} F^{-1}_{Bb} \sigma^{\text{dev}}_{ab} - pJ F^{-1}_{Aa} F^{-1}_{Ba} =: S'_{AB} - pJC^{-1}_{AB}, \tag{6}$$

i.e., $\boldsymbol{S} = \boldsymbol{S}' - pJ\boldsymbol{C}^{-1}$. Note that this is not the deviatoric-volumetric split of tensor $\boldsymbol{S}$, but results from the deviatoric-volumetric split of the Cauchy stress. It is easily checked that

$$\boldsymbol{S}' : \boldsymbol{C} = 0, \qquad p = \frac{1}{3J}\boldsymbol{S} : \boldsymbol{C}.$$

Using split (6), the conservation of linear momentum (4) becomes

$$-\partial_A(F_{aB}S'_{BA}) + \partial_A(pJF^{-1}_{Aa}) = \rho_0 f_a. \tag{7}$$

2.3. Constitutive model

In the framework of nonlinear continuum damage mechanics, the material behavior is described by means of the Helmholtz free energy, decomposed into volumetric and isochoric contributions. In the model we will consider, the strain energy function is expressed as

$$\Psi(\boldsymbol{C}, D) = \Psi_{\text{vol}}(J) + (1 - D)\,\Psi_{\text{iso}}(\bar{\boldsymbol{C}}), \tag{8}$$

where Ψ_{vol} is the volumetric contribution depending solely on the Jacobian J, and Ψ_{iso} is the isochoric (deviatoric) part of the free energy written in terms of the volume-preserving part of the right Cauchy–Green tensor $\bar{\boldsymbol{C}} = J^{-2/3}\boldsymbol{C}$. Abusing of the notation, we shall write derivatives of Ψ_{iso} with respect to $\boldsymbol{C}$, being clear that in fact Ψ_{iso} is a function of $\bar{\boldsymbol{C}}$. The scalar internal variable $D \in [0, 1]$ denotes the isotropic damage variable, such that $D = 0$ represents the undamaged state and $D = 1$ the fully damaged one. Variables $\boldsymbol{C}$ and D are considered independent.

Remark 2.1. *As it is seen from Eq. (8), $\Psi_{vol}(J)$ is not affected by damage. The continuous damage approach we employ allows for the modeling of diffuse fracture propagation as a result of localization, but opening of these fractures is incompatible with incompressibility. Therefore, some sort of relaxation of incompressibility is needed if localization occurs [32], which could be effectively modeled as a degradation of the bulk modulus κ introduced below (see Remark 2.2). If fact, it is shown in [33] that this degradation should be faster than that of the isochoric component. Thus, assumption (8) in fact prevents from having localization. As said earlier, this is outside the scope of this work.*

Definition (8) of the strain energy function is consistent with the classical Kachanov effective stress concept [1,2] and ensures that only the isochoric response is affected by the degradation process, which is particularly relevant for quasi-incompressible materials [12]. The volumetric contribution provides the penalization that controls incompressibility, whereas the deviatoric contribution governs the damage-induced energy dissipation.

Assuming isothermal processes, the Clausius–Duhem inequality in the reference configuration reads

$$\mathcal{D} = -\dot{\Psi} + \frac{1}{2}\boldsymbol{S} : \dot{\boldsymbol{C}} \geq 0, \tag{9}$$

where $\mathcal{D}$ is the internal dissipation. Hereafter, the superposed dot notation is used to denote the material time derivative with respect to a virtual time evolution process that leads to the quasi-static problem we consider, which can be used for example to apply the external load incrementally, as we consider in our implementation. With the free energy split defined in Eq. (8), its material time derivative is

$$\dot{\Psi} = \frac{\partial \Psi}{\partial \boldsymbol{C}} : \dot{\boldsymbol{C}} + \frac{\partial \Psi}{\partial D}\dot{D} = \frac{\partial \Psi}{\partial \boldsymbol{C}} : \dot{\boldsymbol{C}} - \Psi_{\text{iso}}(\bar{\boldsymbol{C}})\,\dot{D}. \tag{10}$$

Substituting in (9) yields

$$\mathcal{D} = \left(\frac{1}{2}\boldsymbol{S} - \frac{\partial \Psi}{\partial \boldsymbol{C}}\right) : \dot{\boldsymbol{C}} + \Psi_{\text{iso}}(\bar{\boldsymbol{C}})\,\dot{D} \geq 0. \tag{11}$$

Since $\dot{\boldsymbol{C}}$ is arbitrary, following the Coleman–Noll procedure we obtain the constitutive relation

$$\boldsymbol{S} = 2\frac{\partial \Psi}{\partial \boldsymbol{C}} = 2\frac{\partial \Psi_{\text{vol}}}{\partial \boldsymbol{C}} + 2(1-D)\frac{\partial \Psi_{\text{iso}}}{\partial \boldsymbol{C}} =: \boldsymbol{S}_{\text{vol}} + (1-D)\boldsymbol{S}_{\text{iso}}. \tag{12}$$

Using the fact that $\frac{\partial J}{\partial \boldsymbol{C}} = \frac{J}{2}\boldsymbol{C}^{-1}$, from (6) it is observed that the thermodynamic pressure is given by $p := -\frac{\partial \Psi_{\text{vol}}}{\partial J}$, and the volumetric contribution becomes

$$\boldsymbol{S}_{\text{vol}} = 2\frac{\partial \Psi_{\text{vol}}}{\partial \boldsymbol{C}} = 2\frac{\partial \Psi_{\text{vol}}}{\partial J}\frac{\partial J}{\partial \boldsymbol{C}} = -p\,J\,\boldsymbol{C}^{-1}, \tag{13}$$

where the sign convention yields a compressive hydrostatic Cauchy stress $-p\boldsymbol{I}$ in the spatial description, as indicated before.

The decoupled volumetric-isochoric constitutive law can be written as:

$$\boldsymbol{S} = \boldsymbol{S}_{\text{vol}} + \boldsymbol{S}', \tag{14a}$$

$$\boldsymbol{S}_{\text{vol}} = -pJ\boldsymbol{C}^{-1}, \tag{14b}$$

$$p = -\frac{\partial \Psi_{\text{vol}}}{\partial J}, \tag{14c}$$

$$\boldsymbol{S}' = (1-D)\boldsymbol{S}_{\text{iso}}, \tag{14d}$$

$$\boldsymbol{S}_{\text{iso}} = 2\frac{\partial \Psi_{\text{iso}}}{\partial \boldsymbol{C}}. \tag{14e}$$

Despite $\boldsymbol{S}'$ is not a deviatoric tensor, it is often referred to as the deviatoric component of $\boldsymbol{S}$, since when (14a) is transformed to the deformed configuration it corresponds to the volumetric-deviatoric splitting of the Cauchy stress.

It remains to provide expressions for the volumetric and isochoric components of the strain energy function.

Observe that the internal dissipation reduces to

$$\mathcal{D} = \Psi_{\text{iso}}(\bar{\boldsymbol{C}})\,\dot{D} \geq 0, \tag{15}$$

which, together with the fact that $\Psi_{\text{iso}}(\bar{\boldsymbol{C}}) \geq 0$, implies the irreversibility condition for damage, i.e., $\dot{D} \geq 0$.

The main goal of this work is to address nonlinear continuum damage mechanics in the finite strain regime, with particular emphasis on the incompressible limit. The volumetric/deviatoric split of the PK2 stress tensor shown in Eq. (14) is the starting point to develop mixed formulations capable of dealing with these physical problems [13,15]. Several constitutive models for both deviatoric and volumetric components are presented in [13]. Let us just describe the ones which will be applied in this work. Readers are referred to [34,35] for further details on this kind of models.

2.3.1. Deviatoric models

The strain energy density must be written in terms of the strain invariants which are defined for the volume-preserving tensor $\bar{\boldsymbol{C}}$ by

$$\bar{I}_1 = \text{trace}\,\bar{\boldsymbol{C}}, \quad \bar{I}_2 = \frac{1}{2}\left[\left(\text{trace}\,\bar{\boldsymbol{C}}\right)^2 - \text{trace}\left(\bar{\boldsymbol{C}}^2\right)\right] = \text{trace Cof}\,\boldsymbol{C},$$

where Cof $\boldsymbol{C}$ represents the cofactor of $\boldsymbol{C}$, and can be obtained as Cof $\boldsymbol{C} = J^2\boldsymbol{C}^{-1}$.

Let us present a suitable function for the deviatoric component of the strain energy function:

- Neo-Hookean model

  This model results from considering only the first principal invariant, so that

$$\Psi_{\text{iso}}(\bar{I}_1) = \frac{\mu}{2}(\bar{I}_1 - 3), \tag{16}$$

  where $\mu > 0$ is the shear modulus.

2.3.2. Volumetric models

Due to the decoupled form of the mechanical strain energy density, compressibility of the mechanical contribution is accounted for by the volumetric strain energy function. Let us now show a model which depends upon the bulk modulus $\kappa = \frac{2\mu(1+\nu)}{3(1-2\nu)}$, where ν is the Poisson ratio:

- Quadratic [36]

$$\Psi_{\text{vol}}(J) = \frac{\kappa}{2}(J-1)^2; \quad \frac{\partial \Psi_{\text{vol}}}{\partial J} = \kappa(J-1). \tag{17}$$

Remark 2.2. *The volumetric functions can be written as $\Psi_{vol}(J) = \kappa\hat{\Psi}_{vol}$. Therefore, the thermodynamic pressure can be used to obtain a proper way to impose the incompressibility of a hyperelastic material:*

$$p = -\frac{\partial \Psi_{vol}}{\partial J} \quad \Leftrightarrow \quad p = -\kappa \frac{\partial \hat{\Psi}_{vol}}{\partial J} \quad \Leftrightarrow \quad \frac{p}{\kappa} + \frac{\partial \hat{\Psi}_{vol}}{\partial J} = 0. \tag{18}$$

This equation can be applied regardless of the compressibility of the material under study. Observe that in the incompressible limit, when Poisson's ratio $\nu \to 0.5$ (for isotropic materials) then $\kappa \to \infty$ and Eq. (18) reduces automatically to

$$\frac{\partial \hat{\Psi}_{vol}}{\partial J} = 0. \tag{19}$$

Eq. (19) imposes directly that $J = 1$, which is in fact the condition that a material must satisfy to be incompressible in finite strain theory.

2.4. Damage model: Evolution of the damage internal variable

The internal scalar variable $D \in [0, 1]$ represents the material degradation. Its evolution is driven by the damage-driving variable

$$\tau = \sqrt{2\,\Psi_{\text{iso}}(\bar{\boldsymbol{C}})}, \tag{20}$$

following the energy-type criterion originally proposed by Simo and Ju [37,38], and subsequently adopted in Comellas et al. [12], as well as in recent continuum damage frameworks for soft tissue modelling [39].

Damage activation and growth are governed by the Kuhn–Tucker loading/unloading conditions:

$$\dot{D} \;\geq\; 0, \qquad F(\tau, \tau_{\max}) \;\leq\; 0, \qquad \dot{D}\, F(\tau, \tau_{\max}) = 0, \tag{21}$$

where $\tau_{\max}$ denotes the maximum value of τ attained during the loading history, and

$$F(\tau, \tau_{\max}) = G(\tau) - G(\tau_{\max}), \tag{22}$$

is the damage surface expressed in terms of the chosen softening law $G(\cdot)$.

Two evolution laws originally proposed in Comellas et al. [12] are considered in this work. Both depend only on two measurable material parameters: the initial damage threshold τ_0^d and the dissipated fracture energy per unit volume g_f^d. For clarity, they are presented separately below.

2.4.1. Linear softening

The linear softening law is written as

$$D = G(\tau) = \begin{cases} 0, & \tau \leq \tau_0^d, \\ \dfrac{1 - \tau_0^d/\tau}{1+H}, & \tau_0^d < \tau < \tau_\infty, \\ 1, & \tau \geq \tau_\infty, \end{cases} \tag{23}$$

where the parameter H is obtained from the fracture energy condition as

$$H = -\frac{(\tau_0^d)^2}{2g_f^d}, \tag{24}$$

and $\tau_\infty = 2g_f^d/\tau_0^d$. Note that $H < 0$, which guarantees that D reaches unity at a finite value τ_∞ of the driving variable. For the purpose of evaluating the consistent tangent operator, the derivative of D with respect to τ is

$$\frac{\partial D}{\partial \tau} = \begin{cases} 0, & \tau \leq \tau_0^d \text{ or } \tau \geq \tau_\infty, \\ \dfrac{\tau_0^d}{(1+H)\,\tau^2}, & \tau_0^d < \tau < \tau_\infty, \\ 0, & \tau \geq \tau_\infty. \end{cases} \tag{25}$$

2.4.2. Exponential softening

The exponential softening law reads

$$D = G(\tau) = \begin{cases} 0, & \tau \le \tau_0^d, \\ 1 - \dfrac{\tau_0^d}{\tau} \exp\left[- A\left(1 - \dfrac{\tau}{\tau_0^d}\right)\right], & \tau_0^d < \tau < \tau_\infty, \\ 1, & \tau \ge \tau_\infty, \end{cases} \tag{26}$$

where now τ_∞ is chosen large enough and the parameter A is calibrated from the fracture energy g_f^d as

$$A = \left[\frac{g_f^d}{(\tau_0^d)^2} - \frac{1}{2} \right]^{-1}. \tag{27}$$

The derivative of D with respect to τ is

$$\frac{\partial D}{\partial \tau} = \begin{cases} 0, & \tau \le \tau_0^d \text{ or } \tau \ge \tau_\infty, \\ \dfrac{\tau_0^d + A\tau}{\tau^2} \exp\left[- A\left(1 - \dfrac{\tau}{\tau_0^d}\right)\right], & \tau_0^d < \tau < \tau_\infty, \\ 0, & \tau \ge \tau_\infty. \end{cases} \tag{28}$$

In both cases, $D(\tau)$ is an accumulative and irreversible variable, bounded between 0 and 1, and its derivative $\partial D/\partial \tau$ provides the sensitivity required for the consistent linearization of the constitutive model.

Remark 2.3. *In the loading surface in Eq. (22), $G(\tau)$ denotes the selected damage evolution law. For the linear and exponential softening laws adopted here, $G(\tau)$ is continuous and strictly increasing on $[\tau_d^0, \tau_\infty)$. Consequently,*

$$\operatorname{sign}\left(F(\tau, \tau_{\max})\right) = \operatorname{sign}\left(G(\tau) - G(\tau_{\max})\right) = \operatorname{sign}(\tau - \tau_{\max}),$$

and the classical Kuhn–Tucker loading/unloading conditions $\dot{D} \ge 0$, $F \le 0$, $\dot{D}\, F = 0$ are fully equivalent to those obtained with $f(\tau, \tau_{\max}) = \tau - \tau_{\max}$ as in the Simo–Ju formulation [37,38]. Defining F through G is convenient because the damage variable is theoretically expressed as $D = G(\tau)$, while its numerical evaluation naturally enforces irreversibility through $D = G(\tau_{\max})$. This approach simplifies both the history update and the consistent tangent derivation.

From a numerical standpoint, the local algorithm described in Section 3.6 introduces small activation and history tolerances $(\varepsilon_{\text{act}}, \varepsilon_{\text{hist}})$, a clamping of $D \in [0, 1]$, and sets $\partial D/\partial \tau = 0$ during unloading or in saturation. The analytical derivative is used only under active loading. These guards ensure smooth transitions near damage initiation and saturation, while preserving thermodynamic consistency and robust Newton convergence.

Remark 2.4. *The damage model adopted in this work is local and does not include an internal length scale. As a result, once strain softening develops, strain localization and post-localization responses may occur, as is well established in the literature on local damage models. Numerous nonlocal and gradient-enhanced damage models have been developed to avoid mesh-dependency in localization. In Section 3.4 we present an argument explaining why we believe these fixes are* not *required in our case. However, as explained in Remark 2.1, the present work does not aim at modeling localization or achieving mesh-objective energy dissipation. Instead, the focus is on the formulation and numerical assessment of a stabilized mixed method for nearly incompressible finite-strain problems with damage, with particular emphasis on stress accuracy, robustness of the nonlinear solution, and consistent linearization.*

2.5. Boundary value problem

We are now in a position to write the field equations of the formulation. They consist of finding $\boldsymbol{u} : \Omega_0 \longrightarrow \mathbb{R}^{\mathrm{d}}$, $\boldsymbol{S}' : \Omega_0 \longrightarrow \mathbb{R}^{\mathrm{d}} \otimes \mathbb{R}^{\mathrm{d}}$ and $p : \Omega_0 \longrightarrow \mathbb{R}$ such that

$$-\nabla_{\boldsymbol{X}} \cdot (\boldsymbol{S}' \cdot \boldsymbol{F}^T) + \nabla_{\boldsymbol{X}} \cdot (pJ\boldsymbol{F}^{-1}) = \rho_0 \boldsymbol{f}, \tag{29a}$$

$$\frac{p}{\kappa} + \frac{\partial \hat{\Psi}_{\text{vol}}}{\partial J} = 0, \tag{29b}$$

$$\boldsymbol{S}' - 2(1 - D)\frac{\partial \Psi_{\text{iso}}}{\partial \boldsymbol{C}} = \boldsymbol{0}, \tag{29c}$$

$$\boldsymbol{C} = \boldsymbol{F}^T \cdot \boldsymbol{F}, \quad \boldsymbol{F} - \nabla_{\boldsymbol{X}} \boldsymbol{u} = \boldsymbol{I}, \tag{29d}$$

together with the calculation of the damage parameter D described above. It is understood that (29d) allows one to compute $\boldsymbol{C}$ and $\boldsymbol{F}$ in terms of $\boldsymbol{u}$, so that the unknowns of the problem are $\boldsymbol{u}$, p and $\boldsymbol{S}'$. If the material is not incompressible, $\boldsymbol{S}'$ and p can be combined and the unknowns can be taken as $\boldsymbol{u}$ and $\boldsymbol{S}$. Furthermore, if $\boldsymbol{S}$ is expressed in terms of $\boldsymbol{u}$ using (29b)-(29c), we obtain the irreducible formulation, written only in terms of $\boldsymbol{u}$. Finally, if $\boldsymbol{S}'$ is written in terms of $\boldsymbol{u}$ using (29c) but p is kept as an unknown, we obtain the $\boldsymbol{u}p$ formulation, suitable for incompressible materials. Nevertheless, in all the developments below, we will consider in detail the three-field $\boldsymbol{u}p\boldsymbol{S}'$ formulation, and present in a summarized form the $\boldsymbol{u}p$ formulation.

The damage function D depends on $\bar{\boldsymbol{C}}$, as indicated in (20). If $\boldsymbol{S}$ or $\boldsymbol{S}'$ *are not* unknowns of the problem, we consider τ as a function of $\boldsymbol{u}$ through $\boldsymbol{C}$. If $\boldsymbol{S}$ or $\boldsymbol{S}'$ *are* unknowns of the problem, then we may consider that τ depends on $\boldsymbol{S}$, and this requires expressing $\bar{\boldsymbol{C}}$ in terms of $\boldsymbol{S}$ by solving pointwise a nonlinear problem. We shall come back to this point later on.

Obviously, the problem needs to be completed with boundary conditions, of the form:

$$\begin{aligned} \boldsymbol{u} &= \boldsymbol{u}_D \qquad \text{on } \Gamma_{0,D}, \\ \boldsymbol{n}_0 \cdot (\boldsymbol{S} \cdot \boldsymbol{F}^T) &= \boldsymbol{t}_N \qquad \text{on } \Gamma_{0,N}, \end{aligned}$$

where $\Gamma_{0,D}$ and $\Gamma_{0,N}$ are a partition of $\partial\Omega_0$, $\boldsymbol{n}_0$ is the unit outward normal to this boundary and $\boldsymbol{u}_D$ and $\boldsymbol{t}_N$ are given.

2.6. Variational formulation

To write the variational formulation of the problem, let us introduce some notation. As usual, $L^p(\Omega_0)$, $1 \le p < \infty$, denotes the space of functions whose power p (not to be confused with the pressure) of its absolute value is integrable in Ω_0, with $L^\infty(\Omega_0)$ the space of bounded functions in Ω_0. $W^{m,p}(\Omega_0)$ denotes the Sobolev space of functions whose derivatives of order up to m are in $L^p(\Omega_0)$, with the usual notation $W^{m,2}(\Omega_0) \equiv H^m(\Omega_0)$. $H(\mathrm{div}, \Omega_0)$ denotes the space of second order tensors with components in $L^2(\Omega)$ and whose divergence has also components in $L^2(\Omega_0)$. The $L^2(\Omega_0)$-inner product is denoted as $(\cdot,\cdot)$ and the integral of the product of two functions, whenever it makes sense, as $\langle\cdot,\cdot\rangle$, with a subscript to indicate the integration domain if it is not Ω_0. The norm in a functional space X will be denoted as $\|\cdot\|_X$.

Let V, Q and T be, respectively, the proper functional spaces where the displacement, the pressure and the component $\boldsymbol{S}'$ of tensor $\boldsymbol{S}$, solution to the problem, are defined. In general, $V \subset H^1(\Omega_0)^{\mathrm{d}}$, $Q \subset L^2(\Omega_0)$ and $T \subset L^2(\Omega_0)^{\mathrm{d}\times\mathrm{d}}$, although the precise definition of these spaces depends on the constitutive law. Let $V_0 \subset V$ be the space of functions in V that vanish on $\Gamma_{0,D}$. In this case, $X = V \times Q \times T$, and we shall also need $X_0 = V_0 \times Q \times T$. The variational statement of the problem is derived by testing system (29a)–(29c) against arbitrary test functions, $\boldsymbol{v} \in V_0$, $\boldsymbol{T} \in T$ and $q \in Q$. The weak form of the problem reads: find $u = \left[\boldsymbol{u}, p, \boldsymbol{S}'\right] \in X$ such that

$$B_{\mathrm{ups}}(u, v) = L(v) \quad \text{for all } v = [\boldsymbol{v}, q, \boldsymbol{T}] \in X_0, \tag{30}$$

where $B_{\mathrm{ups}}(u, v)$ is a semilinear form defined on $X \times X_0$ as

$$B_{\mathrm{ups}}(u, v) := \left\langle \partial_A v_a, F_{aB} S'_{BA} \right\rangle - \left\langle \partial_A v_a, pJ F^{-1}_{Aa} \right\rangle + \left\langle q, \frac{\partial \hat{\Psi}_{\mathrm{vol}}}{\partial J} \right\rangle + \left\langle q, \frac{p}{\kappa} \right\rangle + \langle T_{AB}, S'_{AB} \rangle - \left\langle T_{AB}, 2(1-D)\frac{\partial \Psi_{\mathrm{iso}}}{\partial C_{AB}} \right\rangle,$$

and $L(v)$ is a linear form defined on X_0 as

$$L(v) := \langle v_a, \rho_0 b_a \rangle + \langle v_a, t_a \rangle_{\Gamma_{0_N}}.$$

Note that, in the way the equations have been written, the problem is not symmetric. In fact, the components of the test function $\boldsymbol{T}$ are not stresses, but strains. However, it is possible to render the problem symmetric as it is explained in [14].

To close problem (30), the expression for the damage index D in terms of $\bar{\boldsymbol{C}}$ needs to be added.

3. Numerical approximation

3.1. Linearization

Let us proceed now to the linearization of problem (30). Let us start writing the original problem (29a)–(29c) as

$$\mathcal{A}_{\mathrm{ups}}(u) = f,$$

where $f = [\rho_0 \boldsymbol{f}, 0, \boldsymbol{0}]$ and $\mathcal{A}_{\mathrm{ups}}(u)$ is a nonlinear differential operator. Let $\bar{u} = [\bar{\boldsymbol{u}}, \bar{p}, \bar{\boldsymbol{S}}']$ be a given guess for $u \in X$, understood as the solution obtained in a given iteration of an iterative process. The correction $\delta u = [\delta\boldsymbol{u}, \delta p, \delta\boldsymbol{S}'] \in X_0$ is computed from the equation

$$\mathcal{L}_{\mathrm{ups}}(\bar{u}; \delta u) = f - \mathcal{A}_{\mathrm{ups}}(\bar{u}), \tag{31}$$

where $\mathcal{L}_{\mathrm{ups}}(\bar{u}; \delta u)$ is linear in δu and depends on $\bar{u}$, obtained from the Newton-Raphson linearization of $\mathcal{A}_{\mathrm{ups}}$. In our case, $\mathcal{A}_{\mathrm{ups}}(u)$ and $\mathcal{L}_{\mathrm{ups}}(\bar{u}; \delta u)$ are given by

$$\mathcal{A}_{\mathrm{ups}}(u) = \left[-\partial_A(F_{aB} S'_{BA}) + \partial_A(pJ F^{-1}_{Aa}), \frac{p}{\kappa} + \frac{\partial \Psi_{\mathrm{vol}}}{\partial J}, S'_{AB} - 2(1-D)\frac{\partial \Psi_{\mathrm{iso}}}{\partial C_{AB}} \right], \tag{32}$$

$$\begin{aligned} \mathcal{L}_{\mathrm{ups}}(\bar{u}; \delta u) = [& -\partial_A(\partial_B \delta u_a \bar{S}'_{BA}) - \partial_A(\bar{F}_{aB} \delta S'_{BA}) + \partial_A(\bar{J}\bar{p}\bar{F}^{-1}_{Bb}\partial_B \delta u_b \bar{F}^{-1}_{Aa}) + \partial_A(\bar{J}\delta p \bar{F}^{-1}_{Aa}) - \partial_A(\bar{J}\bar{p}\bar{F}^{-1}_{Ab}\partial_B \delta u_b \bar{F}^{-1}_{Ba}), \\ & \frac{\delta p}{\kappa} + C^{\tan}_{\mathrm{vol}}(\bar{J})\bar{F}^{-1}_{Aa}\partial_A \delta u_a, \\ & \delta S'_{AB} - C'^{\tan}_{ABCD}\bar{F}_{aC}\partial_D \delta u_a]. \end{aligned} \tag{33}$$

The notation involved in these expressions is as follows. First, the first component of $\mathcal{A}_{\mathrm{ups}}(u)$ and of $\mathcal{L}_{\mathrm{ups}}(\bar{u}; \delta u)$ is a vector, with index a, the second component is a scalar and the third component is a tensor, with indices AB. Secondly, the scalar function $C^{\tan}_{\mathrm{vol}}$ comes from the linearization of $\frac{\partial \hat{\Psi}_{\mathrm{vol}}}{\partial J}$. Finally, $C'^{\tan}_{ABCD}$ are the components of the isochoric tangent tensor, which come from the

linearization of the product $(1-D)\frac{\partial \Psi_{\text{iso}}}{\partial C_{AB}}$. Both $C^{\text{tan}}_{\text{vol}}$ and C'^{tan}_{ABCD} depend on the hyperelastic model employed and the damage function. For the case of neo-Hookean hyperelasticity and Ogden hyperelasticity, they can be found in [12]. Note that, using the expression of the damage-driving variable in (20), we have that

$$\frac{\partial}{\partial C_{AB}}\left[2(1-D)\frac{\partial \Psi_{\text{iso}}}{\partial C_{CD}}\right] = 2(1-D)\frac{\partial^2 \Psi_{\text{iso}}}{\partial C_{AB}\partial C_{CD}} - 2\frac{\partial D}{\partial \tau}\frac{\partial \tau}{\partial C_{AB}}\frac{\partial \Psi_{\text{iso}}}{\partial C_{CD}} = 2(1-D)\frac{\partial^2 \Psi_{\text{iso}}}{\partial C_{AB}\partial C_{CD}} - 2\frac{\partial D}{\partial \tau}\frac{1}{\tau}\frac{\partial \Psi_{\text{iso}}}{\partial C_{AB}}\frac{\partial \Psi_{\text{iso}}}{\partial C_{CD}}.$$

The first term is the hyperelastic tangent tensor multiplied by $1-D$ and the second the contribution from the variability of the damage variable.

The variational form of the linearized problem (31) consists of finding $\delta u \in X_0$ such that

$$B_{\text{ups,lin}}(\bar{u};\delta u, v) = L(v) - B_{\text{ups}}(\bar{u}, v) \quad \text{for all } v \in X_0, \tag{34}$$

where the linear form $B_{\text{ups,lin}}(\bar{u};\delta u, v)$ is given by

$$\begin{aligned} B_{\text{ups,lin}}(\bar{u};\delta u, v) = {} & \left\langle \partial_A v_a, \partial_B \delta u_a \bar{S}'_{BA} \right\rangle + \left\langle \partial_A v_a, \bar{F}_{aB}\delta S'_{BA} \right\rangle - \left\langle \partial_A v_a, \bar{J}\bar{p}\bar{F}^{-1}_{Bb}\partial_B \delta u_b \bar{F}^{-1}_{Aa} \right\rangle + \left\langle \partial_A v_a, \bar{J}\bar{p}\bar{F}^{-1}_{Ab}\partial_B \delta u_b \bar{F}^{-1}_{Ba} \right\rangle \\ & - \left\langle \partial_A v_a, \bar{J}\delta p \bar{F}^{-1}_{Aa} \right\rangle + \left\langle q, \frac{\delta p}{\kappa} \right\rangle + \left\langle q, C^{\text{tan}}_{\text{vol}}(\bar{J})\bar{F}^{-1}_{Aa}\partial_A \delta u_a \right\rangle + \langle T_{AB}, S'_{AB}\rangle - \langle T_{AB}, C'^{\text{tan}}_{ABCD}F_{aC}\partial_D \delta u_a\rangle. \end{aligned} \tag{35}$$

3.2. Galerkin finite element approximation

The linear problem (34) can now be approximated using the FE method. For simplicity, let us assume that Ω_0 is a polyhedral domain for which we can consider a family of FE partitions $\mathcal{T}_h = \{K\}$, where K denotes a generic FE domain, h_K its diameter and $h = \max_K\{h_K\}$ the mesh size. All FE functions will be identified with the subscript h. We will consider the same interpolation order for all the elements, although different interpolation orders for the different components of u may be employed. All approximations we shall consider are conforming, i.e., the FE spaces will be chosen as finite dimensional subspaces of the functional spaces where the problem is posed; the important case of discontinuous Galerkin approximations is thus excluded. From $\mathcal{T}_h$ we may construct approximation spaces for the displacement $V_h \subset V$, the pressure $Q_h \subset Q$ and the stress $T_h \subset T$, and from them we can construct $X_h \subset X$ and $X_{0,h} \subset X_0$. We will also be interested in cases in which the test functions belong to the same space as the unknown.

The Galerkin FE approximation to problem (34) consists of finding $\delta u_h \in X_{0,h}$ such that

$$B_{\text{ups,lin}}(\bar{u}_h;\delta u_h, v_h) = L(v_h) - B_{\text{ups}}(\bar{u}_h, v_h) \quad \text{for all } v_h \in X_{0,h}, \tag{36}$$

where $\bar{u}_h \in X_h$ is a given guess for $u_h \in X_h$, obtained from the previous iteration of the Newton-Raphson iterative loop.

Problem (36) is well posed if the following condition holds (see, e.g., [40]):

$$\inf_{u_h \in X_h \setminus \{0\}} \sup_{v_h \in X_{0,h}\setminus\{0\}} \frac{B_{\text{ups,lin}}(\bar{u}_h; u_h, v_h)}{\|u_h\|_X \|v_h\|_X} \geq K_B > 0, \tag{37}$$

for a certain constant K_B and for all $\bar{u}_h \in X_h$. For the formulation we are considering, this condition unfolds into a compatibility condition between the displacement space V_h and the pressure space Q_h, and between the displacement space V_h and the stress space T_h. These conditions are difficult to satisfy and significantly restrict the freedom for the approximation spaces of the different variables. Note also that buckling corresponds to values of $\bar{u}_h$ for which $K_B = 0$. However, we do not consider this possibility in this work.

3.3. Stabilized finite element method

In order to avoid satisfying condition (37), we will use a stabilized FE method based on the VMS concept. We will not elaborate the method here, since the approach is the same as the one described in [14] extended to the case involving damage.

The stabilized counterpart of problem (36) reads as follows: find $\delta u_h \in X_{0,h}$ such that

$$B_{\text{ups,lin}}(\bar{u}_h;\delta u_h, v_h) + \sum_K \langle u', \mathcal{L}^*_{\text{ups}}(\bar{u}_h; v_h)\rangle_K = L(v_h) - B_{\text{ups}}(\bar{u}_h, v_h) \quad \text{for all } v_h \in X_{0,h}, \tag{38}$$

where $\mathcal{L}^*_{\text{ups}}$ is the formal adjoint of operator $\mathcal{L}_{\text{ups}}$ and u' is the so called sub-grid scale (SGS). The former is given by (see [14]):

$$\begin{aligned} \mathcal{L}^*_{\text{ups}}(\bar{u}; v) = [& -\partial_A(\partial_B(v_a \bar{S}'_{AB})) + \partial_A(\bar{J}\bar{p}\bar{F}^{-1}_{Aa}\partial_B v_b \bar{F}^{-1}_{Bb}) - \partial_A(C^{\text{tan}}_{\text{vol}}(\bar{J})q\bar{F}^{-1}_{Aa}) - \partial_A(\bar{J}\bar{p}\bar{F}^{-1}_{Ba}\partial_B v_b \bar{F}^{-1}_{Ab}) + \partial_D(T_{AB}C'^{\text{tan}}_{ABCD}\bar{F}_{aC}), \\ & \frac{q}{\kappa} - \bar{J}\bar{F}^{-1}_{Aa}\partial_A v_a, \\ & \bar{F}_{aB}\partial_A v_a + T_{AB}]. \end{aligned} \tag{39}$$

It remains to define the calculation of the SGS u', which we compute at each iteration and within each element K as:

$$u' = \tau_K P_h^{\perp}(f - \mathcal{A}_{\text{ups}}(\bar{u}_h) - \mathcal{L}_{\text{ups}}(\bar{u};\delta u)), \tag{40}$$

with $P_h^{\perp}$ the $L^2(\Omega_0)$ projection orthogonal to the FE space and

$$\tau_K = \begin{bmatrix} c_1\frac{h_K^2}{\mu_K} & 0 & 0 \\ 0 & c_2\mu_K & 0 \\ 0 & 0 & c_2\mu_K \end{bmatrix}. \tag{41}$$

In this expression, μ_K is a characteristic value of the tangent constitutive tensor in element K (typically the shear modulus) and c_1 and c_2 are algorithmic constants that depend on the polynomial order of the interpolation.

Problem (38) can be solved as it is written, and it provides stable and accurate numerical approximations. However, similar results are obtained if only the terms that really contribute to stability are kept in the product $u'\mathcal{L}^*_{\text{ups}}(\bar{u}_h; v_h)$, leading to what we call the Split-Orthogonal SGS (S-OSGS) formulation. See [13,14] and references therein for further details about this fact, the design of the stabilization parameters and the treatment of the orthogonal projection $P_h^{\perp}$.

3.4. A formulation with improved stress rate of convergence

What we have presented so far is an approximation to the $\boldsymbol{upS'}$ formulation applied to continuum damage and using the standard functional setting, namely, the displacement components belong to $H^1(\Omega_0)$ and the stress components, including the pressure, belong to $L^2(\Omega_0)$. Let us discuss an implication of this fact in the context of damage models.

Suppose that we consider a uniform mesh of size h. If Ω_0 has a re-entrant corner, the regularity for $\boldsymbol{u}$ that we can expect is that $\boldsymbol{u} \in H^{1+s}(\Omega_0)^{\text{d}}$, with $1/2 < s < 1$. Thus, the best convergence estimate for $\boldsymbol{u}$ that we can expect is that

$$\|\boldsymbol{u} - \boldsymbol{u}_h\|_{L^2(\Omega_0)} \lesssim h^{1+s}\|\boldsymbol{u}\|_{H^{1+s}(\Omega_0)}, \tag{42}$$

where $\lesssim$ stands for $\leq$ up to constants. We do not have any analysis of the problem, but definitely it will not be possible to obtain any estimate better than (42), which is the interpolation estimate. Note that this is independent of the polynomial order of interpolation, since it is limited by the regularity of $\boldsymbol{u}$.

Since both $\boldsymbol{S'}$ and p depend on derivatives of $\boldsymbol{u}$, the reconstructed PK2 tensor will depend on derivatives of $\boldsymbol{u}$. The best we can expect is that $\boldsymbol{S}$ has components in $H^s(\Omega_0)$, and therefore the best convergence we can expect for $\boldsymbol{S}$ is

$$\|\boldsymbol{S} - \boldsymbol{S}_h\|_{L^2(\Omega_0)} \lesssim h^s\|\boldsymbol{S}\|_{H^s(\Omega_0)}.$$

The damage variable is a function of tensor $\boldsymbol{C}$, which can be expressed in terms of $\boldsymbol{S}$ by inverting *locally* the constitutive law. Thus, for the following reasoning we may consider our constitutive law as stress driven. Since this constitutive law *needs to be evaluated point-wise*, we need to have point-wise convergent stresses. This amounts to finding r such that $S_{AB} \in W^{r,\infty}(\Omega_0)$ for all components A, B. If this regularity condition holds, the best point-wise error estimate we may expect is

$$\|\boldsymbol{S} - \boldsymbol{S}_h\|_{L^\infty(\Omega_0)} \lesssim h^r\|\boldsymbol{S}\|_{W^{r,\infty}(\Omega_0)}.$$

We are not aware of any result of this type for the complex problem we are dealing with, but it is the best we can expect.

Since $S_{AB} \in H^s(\Omega_0) \equiv W^{s,2}(\Omega_0)$, the question is for which r can we guarantee that $S_{AB} \in W^{r,\infty}(\Omega_0)$. The answer is provided by Sobolev's embedding theorem (see, e.g., [40]), that establishes that this holds if

$$2(s-r) > \text{d} \iff r < s - \frac{\text{d}}{2} \leq s - 1.$$

Since $s < 1$, then $r < 0$. Thus, *stresses cannot converge point-wise* and there is no guaranty that the constitutive law will be evaluated by convergent stresses at points where the displacements are only in $H^{1+s}(\Omega_0)$, which is for example where fracture is prone to occur.

At least for the linear problem and using the displacement-stress formulation, the solution proposed in [17] and subsequent works is to work with a formulation originally analyzed in [41] for the Darcy problem, which requires the stress tensor to have *the divergence in* $L^2(\Omega_0)^{\text{d}}$, i.e., the stress tensor must belong to $H(\text{div};\Omega_0)$. Stress convergence can be improved by a factor 1/2 at the expense of reducing the convergence rate of the displacements also by a factor 1/2. This is mid-way between the primal and the dual formulations (in the latter, the stress convergence rate would be improved by a factor 1 and the displacement convergence rate reduced by a factor 1). Furthermore, essential boundary conditions can still be applied to the displacements, not to the normal stresses, as in the dual formulation. For continuous equal interpolations for all the unknowns, this approach only requires a change in the expression of the stabilization parameters given in (41), without the need to redefine the semilinear form of the problem. See [17,41] for details.

The extension of this idea to the problem we are considering faces two major obstacles:

- The problem we consider is nonlinear.
- We consider as independent unknowns p and $\boldsymbol{S'}$, and we are not aware of any analysis of a dual formulation in this case.

In [19] it was shown that this approach is effective in producing point-wise convergent stresses if pressure and deviatoric stresses are taken as unknowns, even if we do not have any mathematical analysis supporting this fact. The extension of this idea to localization problems with finite strains needs to be further explored, and it is not the objective of this paper (see Remark 2.1).

The major changes to be implemented are that the damage parameter needs to be computed from the stresses and a different way to compute the matrix of stabilization parameters. Within each nonlinear iteration and at each numerical integration point of the FE mesh, the calculations to be performed are:

- From $\bar{p}_h$ and $\bar{\boldsymbol{S}}'_h$, reconstruct the PK2 tensor of the previous iteration $\bar{\boldsymbol{S}}_h$.
- Compute a right Cauchy-Green tensor $\widehat{\boldsymbol{C}}_h$ by solving the discrete counterpart of Eq. (43), namely:

$$\frac{\partial \Psi_{\text{vol}}}{\partial \widehat{\boldsymbol{C}}_h}(\widehat{\boldsymbol{C}}_h) + 2(1-\bar{D}_h)\frac{\partial \Psi_{\text{iso}}}{\partial \widehat{\boldsymbol{C}}_h}(\widehat{\boldsymbol{C}}_h) = \bar{\boldsymbol{S}}_h. \tag{43}$$

  Far enough from bifurcation points this equation will be locally invertible.

- Compute the damage-driving variable in (20) using $\widehat{\boldsymbol{C}}_h$ instead of $\bar{\boldsymbol{C}}_h$.
- Obtain the damage coefficient from $\widehat{\boldsymbol{C}}_h$, say $\widehat{D}_h$.
- Solve problem (38) using $\delta\boldsymbol{u}_h$, δp_h and $\delta\boldsymbol{S}'_h$ as unknowns, but with the damage coefficient $\widehat{D}_h$ and the stabilization matrix computed as

$$\tau_K = \begin{bmatrix} c_1 \frac{h_K \ell}{\mu_K} & 0 & 0 \\ 0 & c_2 \mu_K \frac{h_K}{\ell} & 0 \\ 0 & 0 & c_2 \mu_K \frac{h_K}{\ell} \end{bmatrix}, \tag{44}$$

where ℓ is a characteristic length of Ω_0.

Although the main concern of this work is the improved calculation of stresses in the context of damage, the discussion above justifies that it could be convenient to use as unknown a strain measure, either the right Cauchy-Green tensor $\boldsymbol{C}$, the deformation gradient $\boldsymbol{F}$ or even the Green-Lagrange strain tensor $\boldsymbol{E}$, which has not appeared in the model. This would avoid the need for solving the nonlinear Eq. (43), as the damage-driving variable in (20) could be computed directly with an interpolated unknown of the problem. In our approach, the damage evolution is driven solely by the isochoric strain energy via $\tau = \sqrt{2\,\Psi_{\text{iso}}(\bar{\boldsymbol{C}})}$, ensuring objectivity by construction. Stress-based routes relying on $\mathbf{S}'$, as mentioned above, are considered only as potential extensions and are not employed here.

In this paper we focus on improving the stress *accuracy* by introducing the stress as unknown of the problem, but we wished to clarify the interest of improving the stress *rate of convergence* and the problems in which this can be useful.

3.5. The displacement-pressure formulation

The claim that the introduction of stresses as unknowns improves the accuracy of the solution requires a comparison between the formulation we propose and the one in which stresses are expressed in terms of displacements. Since pressure is required to deal with purely incompressible materials, we will compare the displacement-pressure-stress ($\boldsymbol{up}\boldsymbol{S}'$) formulation described so far with the displacement-pressure ($\boldsymbol{up}$) approach.

We will not detail the steps to arrive at the $\boldsymbol{up}$ formulation here. In the case without damage, this exercise can be found in [14]. Instead, we simply provide the equations to be solved. In all equations below, it is understood that the isochoric stress tensor is expressed in terms of the displacements using the constitutive law in (14e) point-wise.

The counterpart of the continuous nonlinear problem (45) is now: find $u = [\boldsymbol{u}, p] \in X = V \times Q$ such that

$$B_{\text{up}}(u, v) = L(v) \quad \text{for all } v = [\boldsymbol{v}, q] \in X_0 = V_0 \times Q, \tag{45}$$

where the semilinear form $B_{\text{up}}(u, v)$ is given by:

$$B_{\text{up}}(u, v) := \left\langle \partial_A v_a, F_{aB} S'_{BA} \right\rangle - \left\langle \partial_A v_a, pJ F^{-1}_{Aa} \right\rangle + \left\langle q, \frac{\partial \hat{\Psi}_{\text{vol}}}{\partial J} \right\rangle + \left\langle q, \frac{p}{\kappa} \right\rangle. \tag{46}$$

If we write the original nonlinear differential equations as $\mathcal{A}_{\text{up}}(u) = f$, its linearized form can be written as

$$\mathcal{L}_{\text{up}}(\bar{u}; \delta u) = f - \mathcal{A}_{\text{up}}(\bar{u}), \tag{47}$$

where

$$\mathcal{A}_{\text{up}}(u) = \left[-\partial_A (F_{aB} S'_{BA}) + \partial_A (pJ F^{-1}_{Aa}), \frac{p}{\kappa} + \frac{\partial \hat{\Psi}_{\text{vol}}}{\partial J} \right], \tag{48}$$

$$\begin{aligned} \mathcal{L}_{\text{up}}(\bar{u}; \delta u) = [& -\partial_A (\partial_B \delta u_a \bar{S}'_{BA}) - \partial_A (\bar{F}_{aB} \delta S'_{BA}) + \partial_A (\bar{J} \bar{p} \bar{F}^{-1}_{Bb} \partial_B \delta u_b \bar{F}^{-1}_{Aa}) + \partial_A (\bar{J} \delta p \bar{F}^{-1}_{Aa}) - \partial_A (\bar{J} \bar{p} \bar{F}^{-1}_{Ab} \partial_B \delta u_b \bar{F}^{-1}_{Ba}), \\ & \frac{\delta p}{\kappa} + C^{\tan}_{\text{vol}}(\bar{J}) \bar{F}^{-1}_{Aa} \partial_A \delta u_a]. \end{aligned} \tag{49}$$

The variational form of the linearized problem is: find $\delta u = [\delta \boldsymbol{u}, \delta p] \in X_0$ such that

$$B_{\text{up,lin}}(\bar{u}; \delta u, v) = L(v) - B_{\text{up}}(\bar{u}, v) \quad \text{for all } v \in X_0, \tag{50}$$

where

$$\begin{aligned} B_{\text{up,lin}}(\bar{u}; \delta u, v) = & \left\langle \partial_A v_a, \partial_B \delta u_a \bar{S}'_{BA} \right\rangle + \left\langle \partial_A v_a, \bar{F}_{aB} \delta S'_{BA} \right\rangle - \left\langle \partial_A v_a, \bar{J} \bar{p} \bar{F}^{-1}_{Bb} \partial_B \delta u_b \bar{F}^{-1}_{Aa} \right\rangle + \left\langle \partial_A v_a, \bar{J} \bar{p} \bar{F}^{-1}_{Ab} \partial_B \delta u_b \bar{F}^{-1}_{Ba} \right\rangle \\ & - \left\langle \partial_A v_a, \bar{J} \delta p \bar{F}^{-1}_{Aa} \right\rangle + \left\langle q, \frac{\delta p}{\kappa} \right\rangle + \left\langle q, C^{\tan}_{\text{vol}}(\bar{J}) \bar{F}^{-1}_{Aa} \partial_A \delta u_a \right\rangle. \end{aligned} \tag{51}$$

Once the continuous problem is linearized, we can proceed to its FE approximation. In this case, stabilization is required if one wants to avoid the inf-sup condition between spaces V_h and Q_h. This problem is much better understood than finding a triplet $V_h \times Q_h \times T_h$ that is inf-sup stable for the $\boldsymbol{up}\boldsymbol{S}'$ formulation, but nevertheless we also favor a stabilized formulation that allows one to use arbitrary interpolations to construct V_h and Q_h. Assuming that these interpolations are continuous, the discrete linearized problem reads: find $\delta u_h = [\delta \boldsymbol{u}_h, \delta p_h] \in X_{h,0}$ such that

$$B_{\text{up,lin}}(\bar{u}_h; \delta u_h, v_h) + \sum_K \langle u', \mathcal{L}^*_{\text{up}}(\bar{u}_h; v_h) \rangle_K = L(v_h) - B_{\text{up}}(\bar{u}_h, v_h) \quad \text{for all } v_h \in X_{h,0},$$

where the formal adjoint of operator $\mathcal{L}_{\text{up}}$ is given by

$$\mathcal{L}^*_{\text{up}}(\bar{u};v) = [-\partial_A(\partial_B(v_a\bar{S}'_{AB})) + \partial_A(\bar{J}\bar{p}\bar{F}^{-1}_{Aa}\partial_B v_b\bar{F}^{-1}_{Bb}) - \partial_A(C^{\tan}_{\text{vol}}(\bar{J})q\bar{F}^{-1}_{Aa}) - \partial_A(\bar{J}\bar{p}\bar{F}^{-1}_{Ba}\partial_B v_b\bar{F}^{-1}_{Ab}), \frac{q}{\kappa} - \bar{J}\bar{F}^{-1}_{Aa}\partial_A v_a]. \tag{52}$$

The SGSs within each element are computed as

$$u' = \tau_K P^{\perp}_h(f - \mathcal{A}_{\text{up}}(\bar{u}_h) - \mathcal{L}_{\text{up}}(\bar{u};\delta u)), \tag{53}$$

with the matrix of stabilization parameters being

$$\tau_K = \begin{bmatrix} c_1\frac{h_K^2}{\mu_K} & 0 \\ 0 & c_2\mu_K \end{bmatrix}. \tag{54}$$

3.6. Algorithm for the update of the damage variable

As indicated before, we consider a quasi-static time process in which the external loads are applied incrementally. The evaluation of the damage internal variable requires the introduction of a local algorithm to be executed at each numerical integration point (which we call Gauss point in the following) within every nonlinear iteration. This algorithm is responsible for updating the history-dependent variables, namely the maximum value of the damage-driving norm $\tau_{\max}$ attained so far, the damage parameter D, and its derivative $\partial D/\partial\tau$. Its design must guarantee the satisfaction of the irreversibility condition $\dot{D} \geq 0$ and the consistent computation of the tangent operators required for the global Newton–Raphson iterations. At the beginning of the simulation, the internal history variable is initialized as $\tau_{\max} = \tau_0^d$, corresponding to the material damage threshold. This ensures that damage remains inactive until the driving norm exceeds its prescribed value.

The procedure is summarized in the flowchart of Fig. 1. At the beginning of the update, the undamaged isochoric free energy is evaluated from the current deformation state, from which the damage-driving variable $\tau = \sqrt{2\Psi_{\text{iso}}}$ is computed. This scalar quantity is then compared with the stored history variable $\tau_{\max}$. If τ does not exceed $\tau_{\max}$, the process corresponds to unloading or reloading and the value of $\tau_{\max}$ is preserved. Otherwise, when $\tau > \tau_{\max}$, the current value of τ is stored as the new $\tau_{\max}$, signaling active loading.

Once the driving norm is updated, the damage parameter is evaluated by means of the selected evolution law, as described in Section 2.4. The computed D is then saturated within the physically admissible bounds $0 \leq D \leq 1$. Next, the derivative $\partial D/\partial\tau$ is determined. This derivative is only meaningful during active loading while $D < 1$, as it quantifies the sensitivity of the degradation to changes in the driving variable and enters the algorithmic tangent operator. In unloading or fully damaged states, the derivative is set to zero.

Finally, the algorithm stores the updated values of the history variables $\tau_{\max}$, D and $\partial D/\partial\tau$ for use in subsequent increments. This guarantees that the damage variable is path-dependent, accumulative, and consistent with the Kuhn–Tucker loading/unloading conditions. In this way, the local update algorithm provides the link between the continuum damage model and the global FE solution scheme, ensuring both thermodynamic consistency and numerical robustness.

When $\partial D/\partial\tau = 0$, as occurs during unloading or when the damage variable reaches saturation, the damage evolution is frozen and the constitutive response locally reduces to a hyperelastic law with fixed degraded stiffness. In these regimes, the consistent tangent operator does not include damage-related terms, which contributes to a stable convergence of Newton-Raphson's iterative scheme.

4. Numerical examples

In this section a series of numerical examples are presented to assess the performance, robustness, accuracy and applicability of the proposed stabilized mixed formulation for nonlinear continuum damage mechanics. The first case is a verification test with a manufactured solution, designed to analyze spatial discretization errors upon mesh refinement. The second example corresponds to a homogeneous uniaxial tension test, aimed at comparing the stress–stretch responses predicted by different damage evolution laws. Finally, the third example is the classical membrane with a circular hole under tension, which provides a demanding benchmark to evaluate stress accuracy, convergence robustness and the behavior of the formulation in the incompressible limit.

Concerning the nonlinear iterative scheme, for all examples a maximum of 10 iterations are set, with a numerical relative tolerance in the $L^2(\Omega_0)$ norm of 10^{-5}. In order to solve the monolithic system of linear equations, we consider direct solvers implemented in the PETSc parallel solver library [42].

For all the numerical examples included next, hyperelastic models are considered fully incompressible, and so the bulk modulus is $\kappa = \infty$ and the Poisson ratio $\nu = 0.5$, unless otherwise specified. The algorithmic parameters are set to $c_1 = 0.1$ and $c_2 = 0.1$. A detailed sensitivity analysis of these parameters for mixed formulations in finite deformations and multiphysics settings can be found in [15,43] for an in-depth discussion. As previously discussed, the nonlinearities in the problem are solved via a Newton-Raphson scheme. Depending on the nonlinearities, the initial guess of the iterative procedure needs to be close enough to the solution to guarantee convergence of the nonlinear iterations. In our case, the load increment is the parameter which controls the evolution of the nonlinear iterations, so we will have to tune it depending on the nonlinearities of each numerical example. Unless otherwise stated, all numerical examples are conducted using 20 load increments.

The stabilization strategy adopted in this work follows previously validated formulations for incompressible elasticity and is kept fixed throughout the study. The focus is therefore placed on the introduction of the deviatoric stress field and its extension to finite-strain damage, rather than on comparisons between different inf-sup stable or stabilized discretizations.

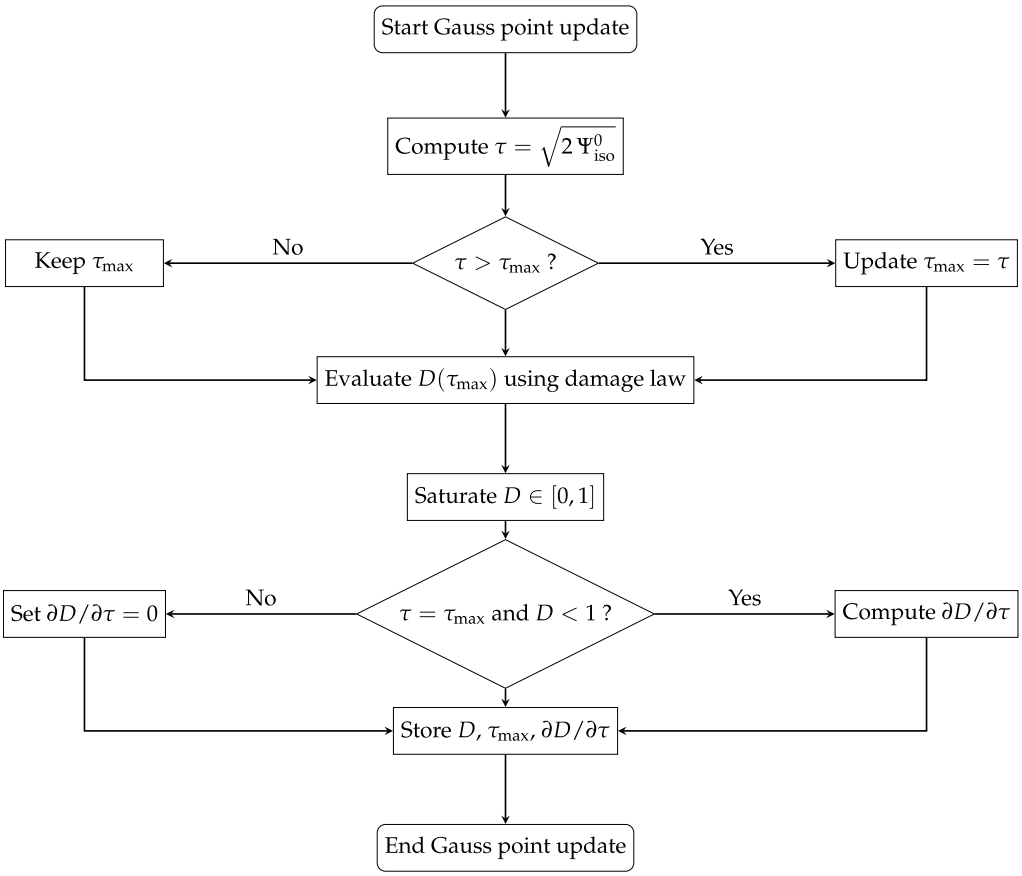

Fig. 1. Flowchart of the damage update algorithm at Gauss point level.

Throughout the formulation, implementation, and post-processing, symmetric second-order tensors are represented using a consistent Voigt mapping. In particular, the same shear weighting is employed in the assembly of the mixed operators, stabilization terms, and in the computation of norms and error measures, ensuring consistency across all stages of the method. With this convention, tensor inner products are preserved under the Voigt representation, i.e. $\mathbf{A} : \mathbf{B} = \boldsymbol{a}^T \boldsymbol{b}$. Symmetry of the deviatoric stress $\mathbf{S}'$ is enforced strongly through the Voigt representation, while deviatoricity with respect to the right Cauchy–Green tensor $\mathbf{C}$ is recovered weakly at convergence of the mixed formulation.

To ensure a fair comparison between the different formulations, we will compare the results with respect to the number of Degrees Of Freedom (DOFs), i.e., the total number of unknowns in the whole algebraic system. All simulations reported in this work are performed using sparse direct solvers from PETSc. The focus is on formulation robustness and solution quality rather than on large-scale solver performance or scalability. The largest system considered in this study involves approximately 10^7 global DOFs. No claim is made regarding computational efficiency in terms of wall-clock time.

4.1. A verification test with a manufactured solution

Let us first perform a simple test whose main objective is to numerically check the order of convergence of the proposed scheme with respect to the mesh size in the presence of finite-strain damage. For this purpose we use the so-called method of manufactured solutions.

In this procedure, an exact analytical solution is defined a priori and later substituted into the continuum equations in order to obtain the associated forcing terms. These forcing terms are then introduced in the FE computation. The manufactured solutions are composed of smooth functions. Dirichlet boundary conditions are prescribed over the boundaries upon evaluation of the displacement analytical solution.

The region we consider is the unit square $\Omega_0 = (0,1) \times (0,1)$ under plane strain assumption and we impose the following manufactured displacement and pressure fields:

$$\mathbf{u}(X,Y) = U\left[\exp(X+Y), -\exp(X+Y)\right], \tag{55}$$

$$p(X,Y) = \mu \sin(2\pi X)\sin(2\pi Y), \tag{56}$$

where $U = 0.01$ and X, Y denote the Cartesian axes in the reference configuration. All quantities are assumed dimensionless in this example. This displacement field corresponds to an incompressible motion, since the Jacobian is $J(X, Y) = 1$ for all X, Y. We set a Neo-Hookean model for the isochoric part of the stresses, with shear modulus $\mu = 3.3 \times 10^6$, and a quadratic law for the volumetric response.

The manufactured damaged isochoric PK2 stress field is now degraded by the isotropic damage variable according to

$$\boldsymbol{S}'(X, Y) = (1 - D)\, \boldsymbol{S}_{\text{iso}}(X, Y). \tag{57}$$

In this test, the linear softening law presented in Section 2.4 is considered, with material parameters $\tau_0^d = 100$ and $g_f^d = 3 \cdot 10^4$. With this choice, the domain contains elastic ($D = 0$) and active ($0 < D < 1$) regions, which makes the test particularly suitable to assess the robustness of the formulation. The body forces and boundary tractions for the manufactured solution are obtained symbolically from the prescribed fields and the damaged constitutive law. The explicit expressions are lengthy and are therefore not reported here. A MATLAB script reproducing the complete derivation is provided as Supplementary Material (SM1).

Dirichlet boundary conditions are prescribed on the entire boundary by imposing the analytical displacement field. No traction boundary conditions are applied. In addition, the pressure field is fixed at a single reference corner point in the domain to remove the null space associated with the incompressible constraint.

We study the convergence behavior of the proposed method by running the case on a sequence of seven uniformly refined meshes. The grids consist of n^2 bilinear (Q1) and biquadratic (Q2) quadrilateral elements, being n the number of FEs along each side of the domain. When referring to Q1 and Q2 discretizations, the same interpolation order is used for all primary variables. Numerical integration is performed using a standard open Gauss–Legendre quadrature rule of sufficient order to consistently integrate the element interpolation, without reduced or selective integration. Errors are computed in the $L^2(\Omega_0)$ norm for the displacement $\mathbf{u}$, the pressure p, and the damaged isochoric PK2 stress $\boldsymbol{S}'$, and are plotted against both the element mesh size h and the number of DOFs.

Fig. 2a shows the displacement convergence rate upon mesh size. As expected, both formulations exhibit a convergence order of $k + 1$, k being the polynomial order of the FE interpolation. With respect to both pressure and damaged isochoric PK2 stress fields, both present the expected convergence order of k upon mesh refinement as it can be observed in Fig. 2c–e. The reader can note that the schemes proposed show the desired rate of convergence.

More interesting results are obtained when comparing these convergence rates with respect to DOFs. Fig. 2b–d show the displacement and pressure convergence rates upon DOFs, respectively. All fields are considered as primary unknowns of both formulations and therefore a similar accuracy for a given mesh size is expected, especially when linear elements are considered. Fig. 2f displays the deviatoric PK2 mechanical stress convergence rates upon DOFs for both formulations. As expected, higher accuracy is achieved for a given mesh size for the mixed $\boldsymbol{up}\boldsymbol{S}'$ formulation. Results clearly show that both the $\boldsymbol{up}\boldsymbol{S}'$ and the $\boldsymbol{up}$ formulations deal appropriately with the incompressibility constraint but the three-field formulation exhibits a higher accuracy in the stress field for linear elements, even for very coarse meshes.

Note that the $\boldsymbol{up}$ formulation computes the stresses (locally) at the numerical integration points, while the $\boldsymbol{up}\boldsymbol{S}'$ formulation adopts a continuous stress field. To compare stress accuracy, a local smoothing technique has been applied to the original discontinuous stress fields of the mixed $\boldsymbol{up}$ formulation. So, Fig. 2e-f display the continuous stress fields obtained after the smoothing operation.

When comparing formulations at equal numbers of global DOFs, it should be noted that the three-field formulation involves additional stress degrees of freedom, so that, for a given algebraic size, the two-field formulation corresponds to a finer spatial discretization. The improved stress accuracy of the proposed formulation becomes apparent once the spatial discretization is sufficiently refined, as the independent stress field can then effectively reduce projection errors associated with displacement-based stress recovery.

4.2. Homogeneous uniaxial tension

The second benchmark corresponds to the homogeneous uniaxial tension test, in the spirit of the study presented in [12]. The objective is to assess the response of the proposed formulation under large stretches and to investigate the influence of different damage evolution laws on the global stress–stretch curves.

The test is defined by subjecting a single hexahedral element to a displacement-driven uniaxial load state. Homogeneous tensile deformation is imposed along one axis, while the remaining directions are constrained to enforce a pure tension state and prevent rigid body motions. Since the imposed kinematics are homogeneous, the resulting stress and strain fields remain uniform, which makes this problem a convenient setting to directly compare the constitutive predictions with the numerical response.

A Neo-Hookean model is adopted for the isochoric part of the strain energy, with shear modulus $\mu = 15$ kPa. The volumetric contribution follows a quadratic law, and incompressibility is assumed. The damage-driving variable is defined according to Section 2.4, with material parameters $\tau_0^d = 57.7\ \sqrt{\text{Pa}}$ and $g_f^d = 20\ \text{kJ/m}^3$. Unless otherwise specified, these values are used in the simulations reported below.

4.2.1. Effect of the damage evolution law

The objective of this example is to analyze the evolution of the main variables of interest under different damage evolution laws. For this purpose, the loading is monotonically increased until the element becomes fully degraded. This setting allows us to directly compare the effect of the linear and exponential softening models on the stress, pressure and damage responses.

Fig. 3 shows the response under homogeneous uniaxial tension for both the linear and exponential softening laws. Panel (a) reports the evolution of the deviatoric PK2 stress with respect to the applied stretch. Both laws coincide in the initial elastic regime

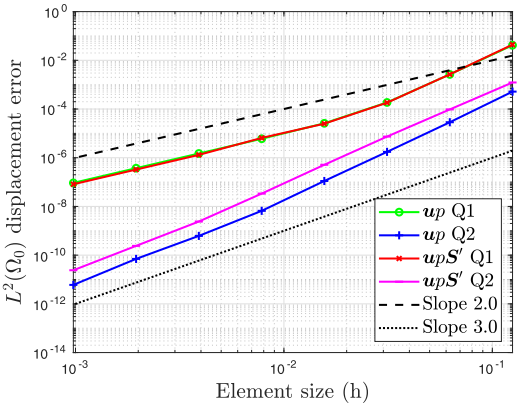

(A) Displacement error upon mesh refinement

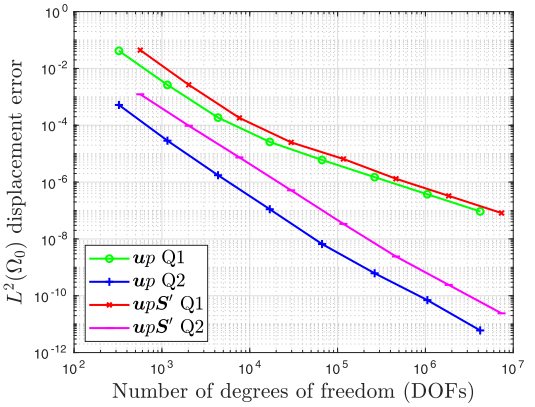

(B) Displacement error upon DOFs

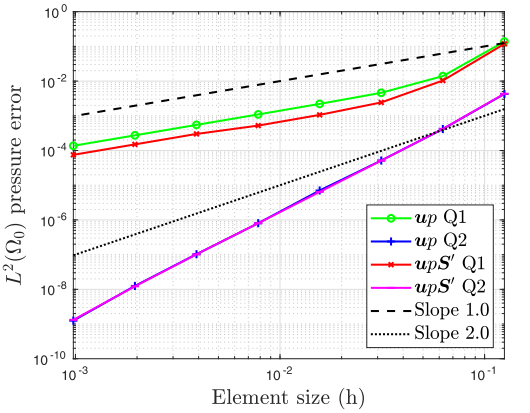

(C) Pressure error upon mesh refinement

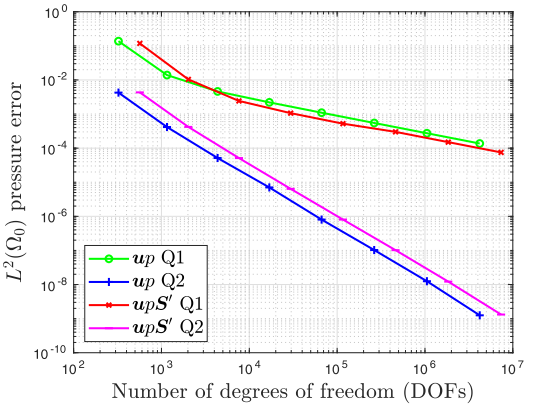

(D) Pressure error upon DOFs

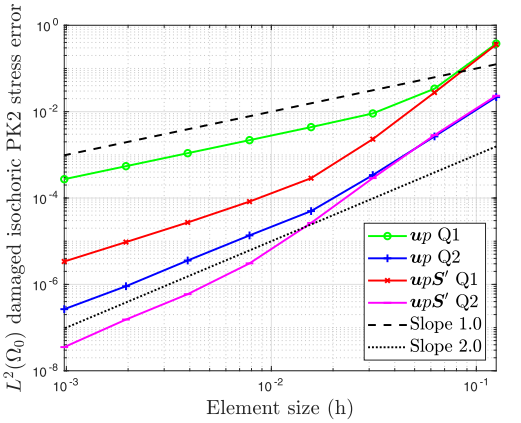

(E) Damaged isochoric PK2 stress error upon mesh refinement

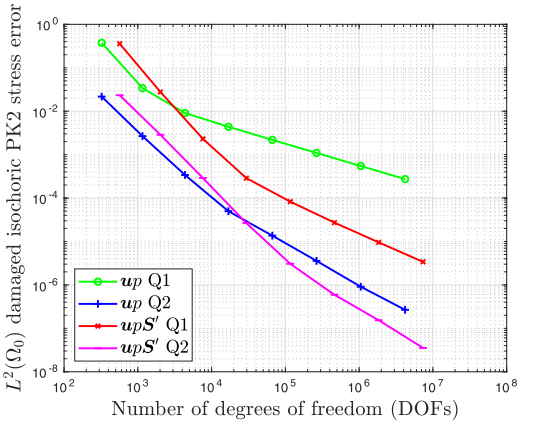

(F) Damaged isochoric PK2 stress error upon DOFs

Fig. 2. A verification test with manufactured solution. Convergence rates for both up and upS' formulations.

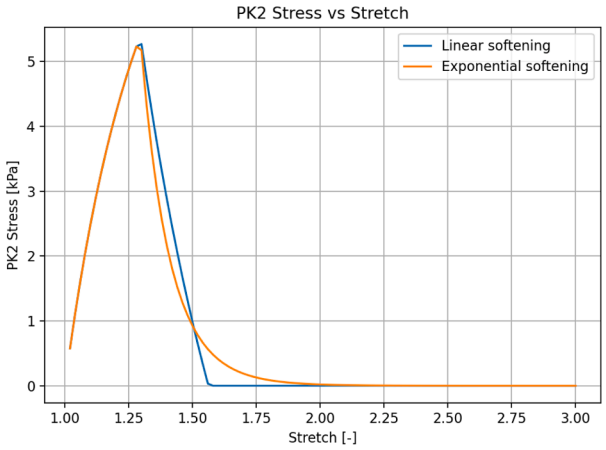

(A) Damaged isochoric PK2 stress (kPa)

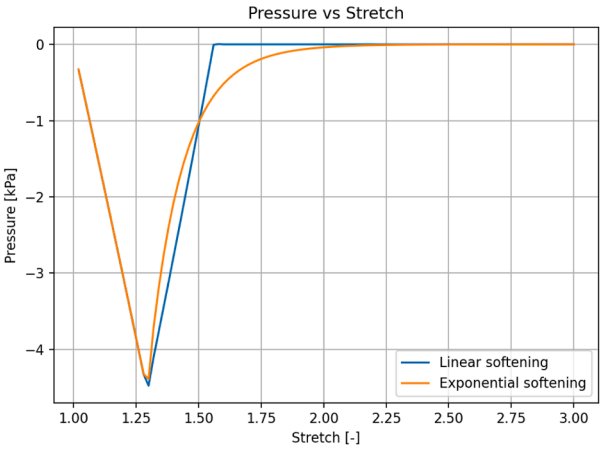

(B) Pressure (kPa)

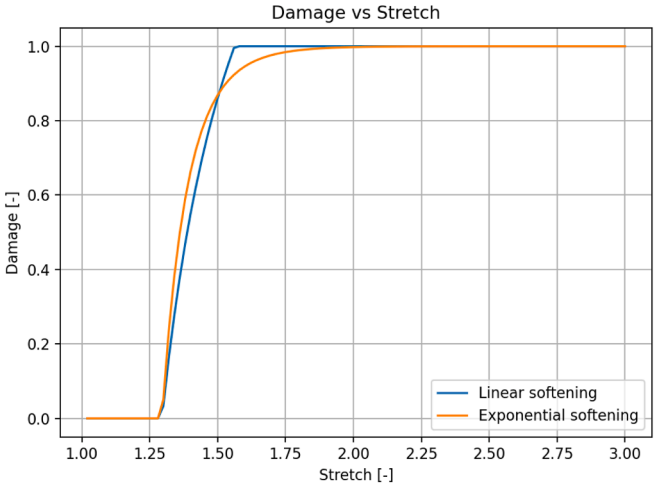

(C) Damage variable (−)

Fig. 3. Homogeneous uniaxial tension. Effect of different damage evolution laws under stretching: (a) deviatoric PK2 stress, (b) pressure, (c) damage variable.

and predict a complete degradation of the deviatoric response as $D \to 1$, but the linear law exhibits a more abrupt softening branch, while the exponential law results in a smoother decay. Panel (b) displays the pressure response, which gradually decreases as damage evolves and vanishes in the fully degraded state, with the exponential law again providing a more progressive transition. Finally, Panel (c) illustrates the monotonic growth of the internal damage variable. Damage initiates at the prescribed threshold $\tau_0^d = 100$ and accumulates irreversibly, with the linear model producing a steeper increase and the exponential law yielding a more gradual evolution. These results highlight the significant influence of the choice of damage evolution law on the macroscopic stress–stretch behavior, while confirming the robustness of the proposed formulation under large homogeneous deformations.

4.2.2. Effect of the initial damage threshold norm

In order to investigate the influence of the initial damage threshold τ_0^d, we perform a cyclic uniaxial tension test consisting of successive loading and unloading phases. The specimen is first stretched up to a prescribed level below the threshold, then unloaded to the reference configuration. A second loading branch is imposed beyond τ_0^d, activating damage, followed by unloading and a final reloading stage. This procedure allows us to highlight the role of τ_0^d on the onset of damage, as well as the irreversible nature of the degradation process upon unloading and reloading.

The initial damage threshold defines the norm of the strain energy at which damage starts to accumulate. Lower values of τ_0^d promote an earlier onset of degradation, while higher values delay the initiation of softening.

Fig. 4 summarizes the results obtained for two representative thresholds, $\tau_0^d = 27.7\ \sqrt{\text{Pa}}$ and $\tau_0^d = 57.7\ \sqrt{\text{Pa}}$, compared against the undamaged reference response. Panel (a) shows the evolution of the deviatoric PK2 stress. As expected, decreasing τ_0^d shifts the

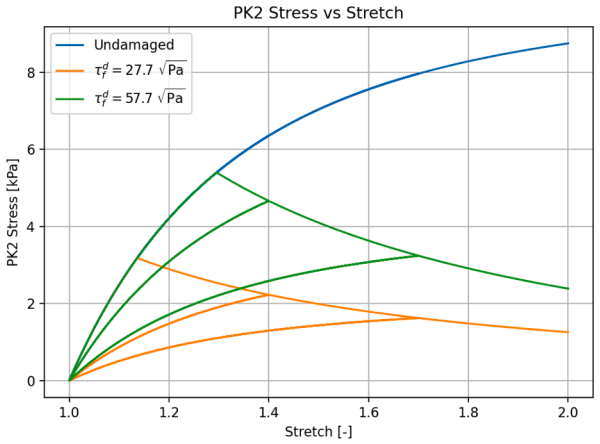

(A) Damaged deviatoric PK2 stress tensor (kPa)

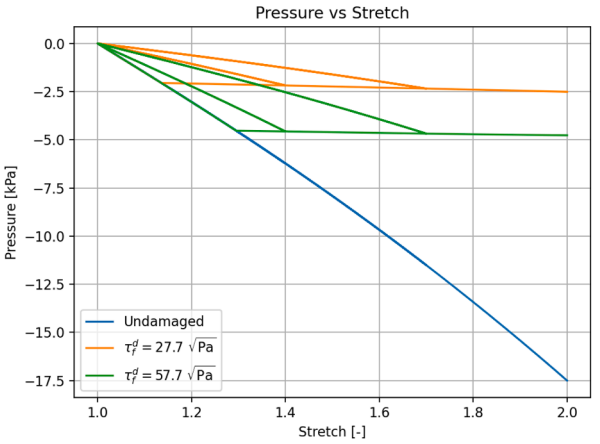

(B) Pressure (kPa)

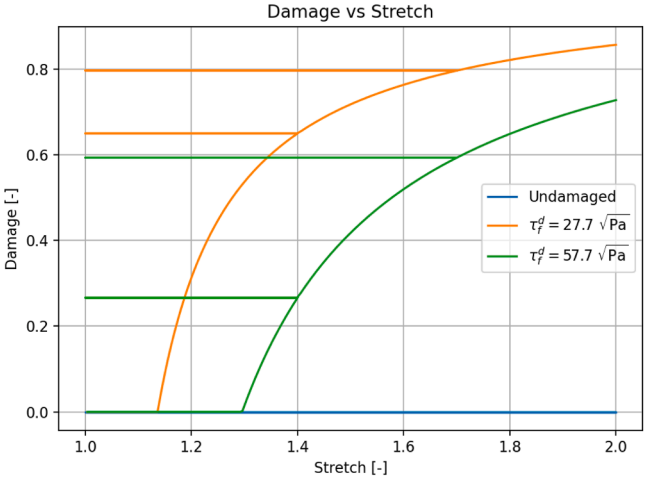

(C) Damage parameter (-)

Fig. 4. Homogeneous uniaxial tension. Influence of different initial damage threshold norms under stretching.

onset of softening to lower stretch values, leading to a faster reduction of the load-carrying capacity. Panel (b) presents the pressure response, which is also affected by the earlier damage activation: the case with $\tau_0^d = 27.7\ \sqrt{\text{Pa}}$ exhibits a smoother pressure decrease than the one with $\tau_0^d = 57.7\ \sqrt{\text{Pa}}$. Finally, Panel (c) illustrates the corresponding evolution of the damage variable D, highlighting that a smaller τ_0^d results in a steeper and earlier growth of damage, while a larger threshold delays and moderates the degradation process. Overall, these results confirm the direct role of the initial threshold norm in controlling the onset of damage and in shaping the subsequent stress–stretch response.

4.2.3. *Effect of the fracture energy per unit volume*

The third parametric study analyzes the influence of the fracture energy per unit volume g_f^d on the softening response. This parameter governs the slope of the degradation law once damage has initiated, and thus controls the rate at which the material loses its load-carrying capacity. Small values of g_f^d produce steep softening branches and a rapid collapse, whereas large values lead to a more gradual reduction of stresses.

Fig. 5 presents the comparison between three representative values, $g_f^d = 3$, 20, and 600 kJ/m^3. Panel (a) shows the deviatoric PK2 stress–stretch curves. The case with $g_f^d = 3$ kJ/m^3 exhibits an abrupt stress drop and reaches full degradation at relatively small stretches, while increasing g_f^d delays and smoothens the softening branch. Panel (b) displays the corresponding pressure evolution, which mirrors the trend observed in the deviatoric stresses. Panel (c) illustrates the damage variable, confirming that higher g_f^d values reduce the growth rate of D and extend the range of stretch over which damage evolves. These results confirm the role of

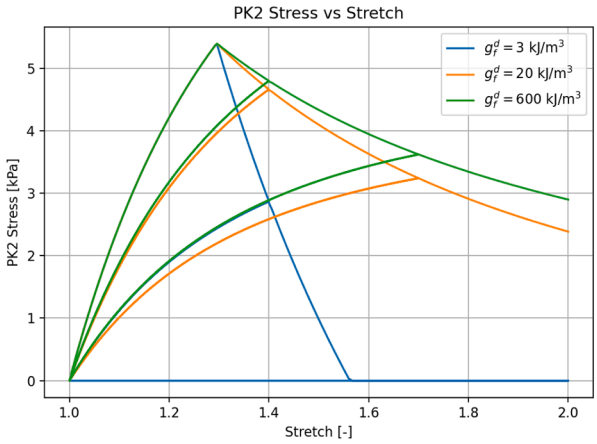

(A) Damaged deviatoric PK2 stress tensor (kPa)

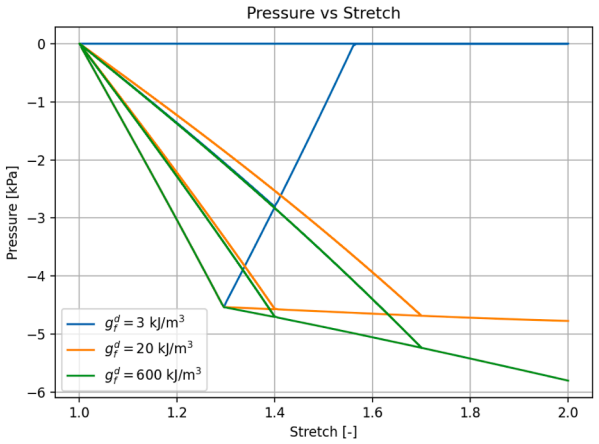

(B) Pressure (kPa)

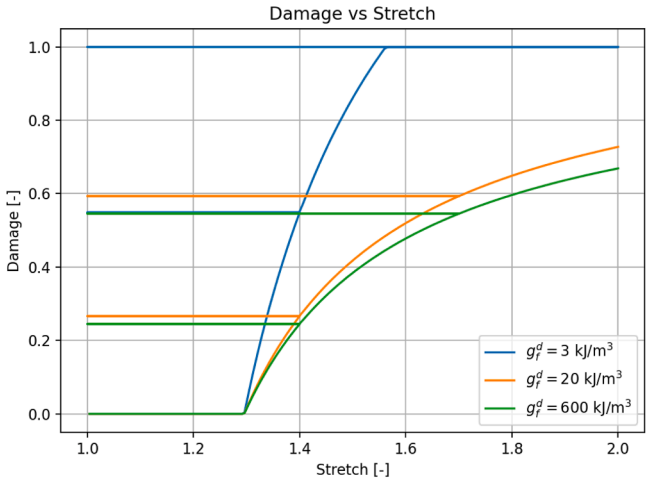

(C) Damage parameter (-)

Fig. 5. Homogeneous uniaxial tension. Influence of different fracture energy per unit volume values under stretching.

the dissipated fracture energy in regularizing the softening process and preventing premature collapse, highlighting its importance in calibrating the constitutive model.

To further assess the robustness of the nonlinear solution procedure, Fig 6 reports the Newton convergence history for selected load steps of the uniaxial tension test, including elastic loading, damage initiation, and the damaged regime. The global residual norm decreases by several orders of magnitude within a small number of iterations for all considered steps. Once damage is activated, the convergence behavior approaches the expected quadratic rate, confirming the effectiveness of the consistent damage tangent employed in the formulation. These results illustrate the stability of the proposed algorithmic treatment without the need for line-search or arc-length techniques, relying solely on adaptive load stepping if required.

The homogeneous uniaxial test demonstrates the robustness of the proposed formulation under finite deformations and highlights the role of the constitutive parameters in controlling the onset and evolution of damage. The comparative study confirms that both the choice of softening law and the calibration of τ_0^d and g_f^d have a direct impact on the stress–stretch response, while the formulation consistently reproduces the expected homogeneous behavior in agreement with [12].

4.3. Membrane with a hole

To assess the robustness of the proposed stabilized three–field formulation and, in particular, its stress accuracy under strong concentration effects, we consider the classical benchmark of a plate with a central circular hole under tension, following a set-up akin to Comellas et al. [12].

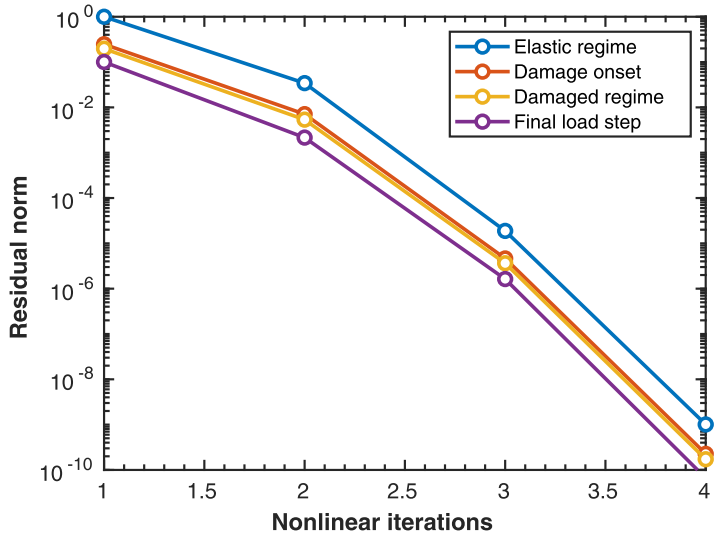

Fig. 6. Homogeneous uniaxial tension. Newton convergence history for selected load steps of the uniaxial tension test, showing the decay of the global residual norm during elastic loading, damage onset, and the damaged regime.

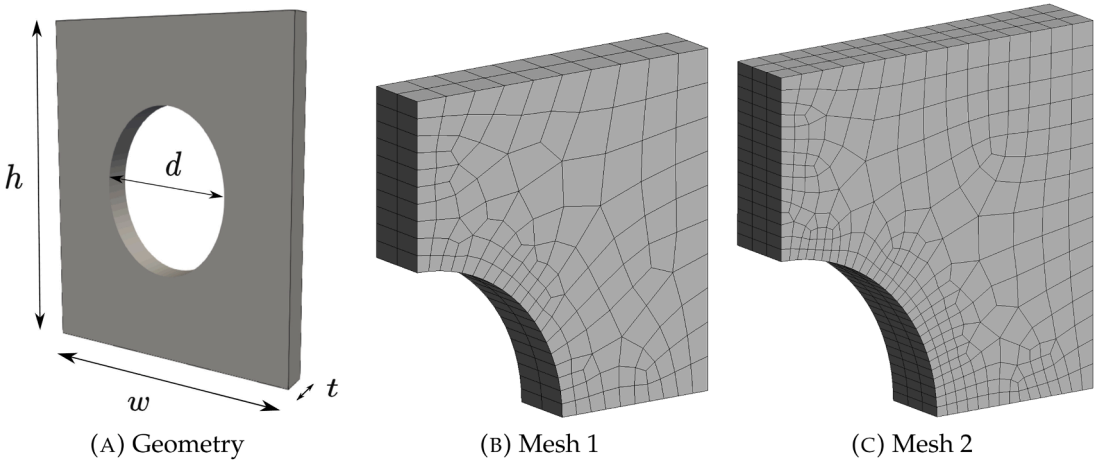

Fig. 7. Membrane with a hole. Geometry and computational meshes.

The specimen is a rectangular plate of width $w = 200$ mm, height $h = 200$ mm and thickness $t = 20$ mm, with a centered cylindrical hole of diameter $d = 100$ mm (Fig. 7a). The loading is displacement controlled: a vertical displacement $u = 85$ mm is prescribed on the top face and an equal displacement of opposite sign on the bottom face, generating an overall tensile stretch. Lateral faces are traction-free; rigid-body motions are prevented by fixing a point on the bottom edge in the loading direction. This configuration induces a pronounced stress concentration in the ligament adjacent to the hole and is therefore demanding in terms of incompressibility handling, nonlinear convergence, and stress prediction. In this case, 100 load steps are set.

The material model follows the volumetric/isochoric split adopted in this work. A quadratic volumetric energy enforces near-incompressibility, whereas the isochoric contribution is Neo–Hookean with shear modulus $\mu = 15$ kPa, degraded by an isotropic damage variable D driven by the energy-type norm described in Section 2.4. A linear softening law is used, with parameters $\tau_0^d = 157.7\ \sqrt{\text{Pa}}$ and $g_f^d = 60\ \text{kJ/m}^3$.

Discretization employs equal-order continuous hexahedra for all unknowns, stabilized with the VMS/S-OSGS terms of Section 3. Owing to symmetry, only a quarter of the domain is modeled and symmetry conditions are imposed on the two mid-planes; the two meshes considered are shown in Fig. 7b-c. For comparison we also solve the displacement–pressure ($\boldsymbol{up}$) formulation on the same meshes. To compare stress accuracy at comparable algebraic cost, the meshes are chosen so that the total number of DOFs is (nearly) matched across formulations: specifically, Mesh 1 with the three-field $\boldsymbol{upS'}$ formulation has practically the same number of DOFs as Mesh 2 with the $\boldsymbol{up}$ formulation. The mesh properties are summarized in Table 1. In this example, the objective is to compare both formulations at comparable algebraic resolution rather than to perform a mesh convergence study. For this reason, mesh M2 for the

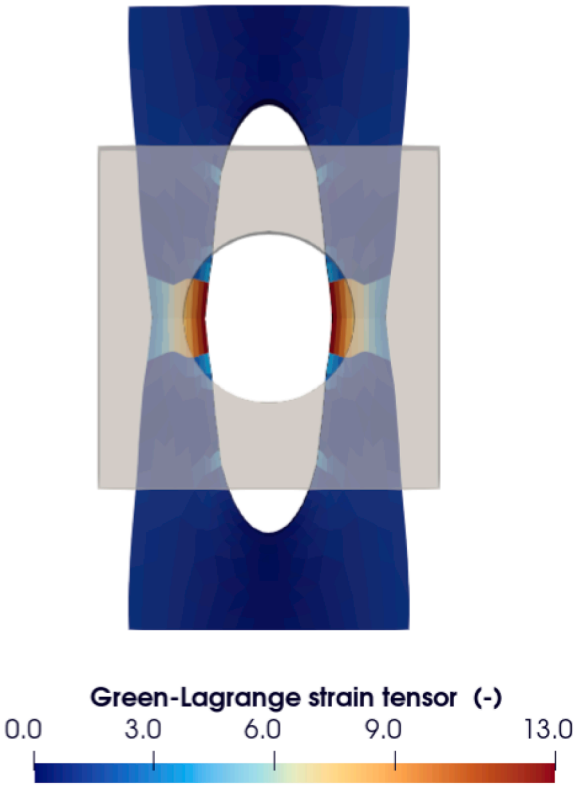

Fig. 8. Membrane with a hole. Green–Lagrange strain field (norm) with initial and deformed configurations.

Table 1
Membrane with a hole. Computational mesh properties.

Mesh	Nodes	Elements	DOFs $\boldsymbol{u}p$	DOFs $\boldsymbol{u}p\boldsymbol{S}'$
M1	525	288	2,100	5,250
M2	1,340	867	5,360	13,400

two-field formulation is designed to have approximately the same number of global degrees of freedom as mesh M1 for the three-field formulation. This allows for a fair comparison of stress accuracy at similar computational cost.

We first provide context by displaying the full specimen (rather than the quarter model) to superpose the initial configuration with the deformed shape at the end of loading, coloured by the norm of the Green–Lagrange strain tensor; see Fig. 8. The largest strains develop in the ligaments around the hole, as expected, and peak values are orders of magnitude larger than 10^{-3}, clearly outside the infinitesimal-strain regime. This confirms the need for a finite-strain formulation. All subsequent analyses exploit symmetry and are performed on a quarter model.

Turning to kinematics, Fig. 9 compares the displacement magnitude at the last load step for $\boldsymbol{u}p$–Mesh 1, $\boldsymbol{u}p$–Mesh 2 and $\boldsymbol{u}p\boldsymbol{S}'$–Mesh 1. All solutions exhibit the same global pattern, with maxima at the free upper corner and strong gradients across the ligament. The coarse $\boldsymbol{u}p$–Mesh 1 field shows mild faceting due to under-resolution, which is mitigated by refinement ($\boldsymbol{u}p$–Mesh 2). Crucially, the three-field $\boldsymbol{u}p\boldsymbol{S}'$ solution on Mesh 1 delivers a displacement field essentially indistinguishable from $\boldsymbol{u}p$ on Mesh 2 at matched DOFs, showing that the proposed mixed formulation preserves global kinematics and that the VMS/S-OSGS stabilization prevents volumetric locking.

Regarding the hydrostatic response, recall that we adopt the convention $\boldsymbol{\sigma} = -p\,\boldsymbol{I} + \boldsymbol{\sigma}^{\mathrm{dev}}$ for the Cauchy stress (i.e., tension corresponds to negative p). The most negative pressures concentrate along the ligament and near the lower free corner, while small positive values appear on the opposite side. On the coarse $\boldsymbol{u}p$ mesh a staircase/banded pattern is noticeable along the ligament, a typical artifact of equal-order $\boldsymbol{u}p$ discretizations under sharp gradients; refinement reduces but does not eliminate the wiggles. In contrast, the three-field $\boldsymbol{u}p\boldsymbol{S}'$ solution on Mesh 1, at essentially the same algebraic cost as $\boldsymbol{u}p$ on Mesh 2, yields a visibly smoother hydrostatic layer around the hole while keeping $J \approx 1$; see Fig. 10.

We finally examine the norm of the damaged deviatoric PK2 stress, $\|\boldsymbol{S}'\| = (1-D)\,\|\boldsymbol{S}_{\mathrm{iso}}\|$ (Fig. 11). The hotspot is confined to the ligament and the lower free corner, with rapid decay away from that region. On the coarse $\boldsymbol{u}p$ mesh, layer-type oscillations aligned with element rows remain visible; refinement attenuates but does not suppress them. By contrast, the $\boldsymbol{u}p\boldsymbol{S}'$ solution on Mesh 1 produces

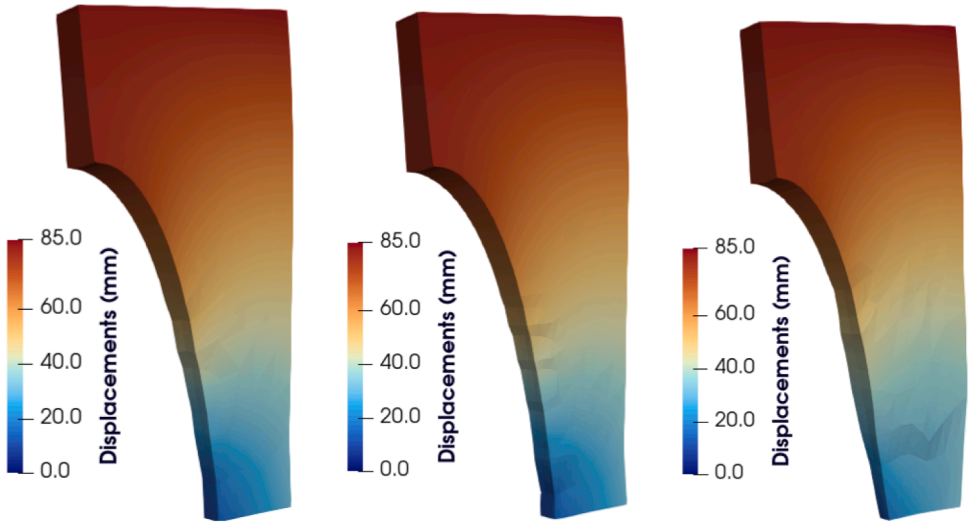

(A) $\boldsymbol{up}$ formulation, Mesh 1

(B) $\boldsymbol{up}$ formulation, Mesh 2

(C) $\boldsymbol{upS'}$ formulation, Mesh 1

Fig. 9. Membrane with a hole. Displacement field (magnitude) for $\boldsymbol{up}$ and $\boldsymbol{upS'}$ formulations.

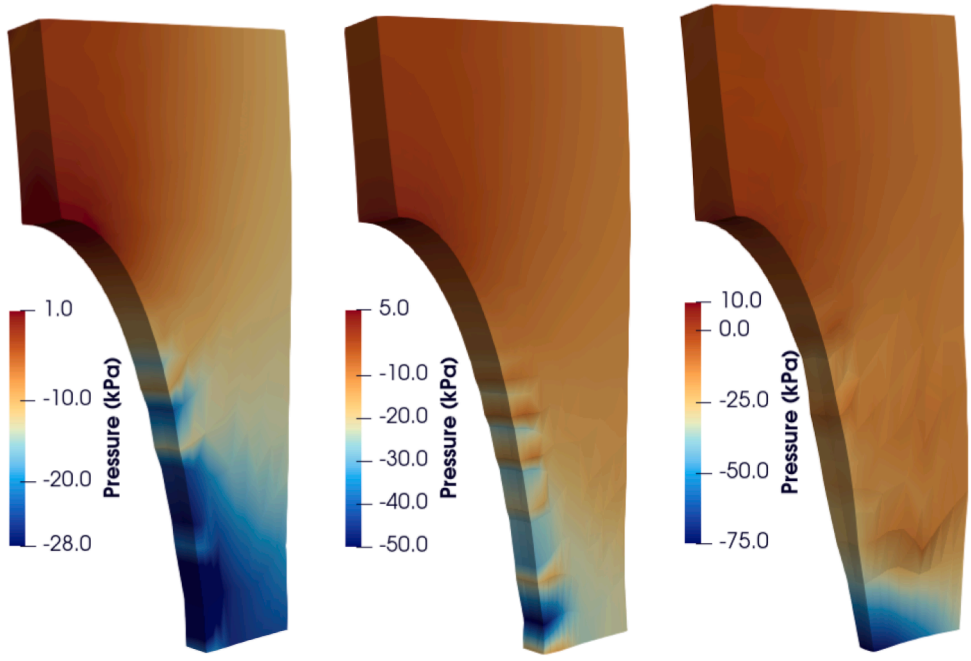

(A) $\boldsymbol{up}$ formulation, Mesh 1

(B) $\boldsymbol{up}$ formulation, Mesh 2

(C) $\boldsymbol{upS'}$ formulation, Mesh 1

Fig. 10. Membrane with a hole. Hydrostatic pressure field p (kPa) for $\boldsymbol{up}$ and $\boldsymbol{upS'}$ formulations.

a compact, smooth hotspot with monotonic radial decay and no checkerboard/banding, at comparable algebraic cost to $\boldsymbol{up}$–Mesh 2. Since the damage driving norm $\tau = \sqrt{2\,\Psi_{\text{iso}}(\bar{\boldsymbol{C}})}$ depends on the isochoric response (and hence on $\boldsymbol{S'}$), the improved regularity of the stress field in $\boldsymbol{upS'}$ translates directly into a cleaner, more mesh-objective damage distribution, as shown in Fig. 12.

At matched DOFs, the three-field $\boldsymbol{upS'}$ formulation reproduces the global kinematics of the $\boldsymbol{up}$ model and prevents volumetric locking. More importantly, it delivers a markedly smoother hydrostatic pressure and a cleaner deviatoric stress hotspot in the ligament, which in turn yields a more robust and mesh-objective damage pattern. The $\boldsymbol{up}$ formulation attains comparable stress quality only after

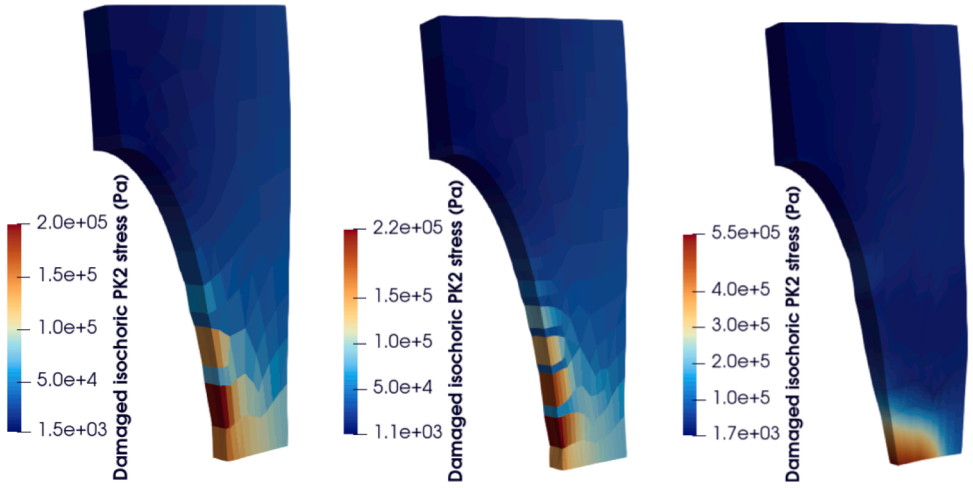

(A) $\boldsymbol{up}$ formulation, Mesh 1 (B) $\boldsymbol{up}$ formulation, Mesh 2 (C) $\boldsymbol{upS'}$ formulation, Mesh 1

Fig. 11. Membrane with a hole. Damaged isochoric PK2 stress (norm) for $\boldsymbol{up}$ and $\boldsymbol{upS'}$ formulations.

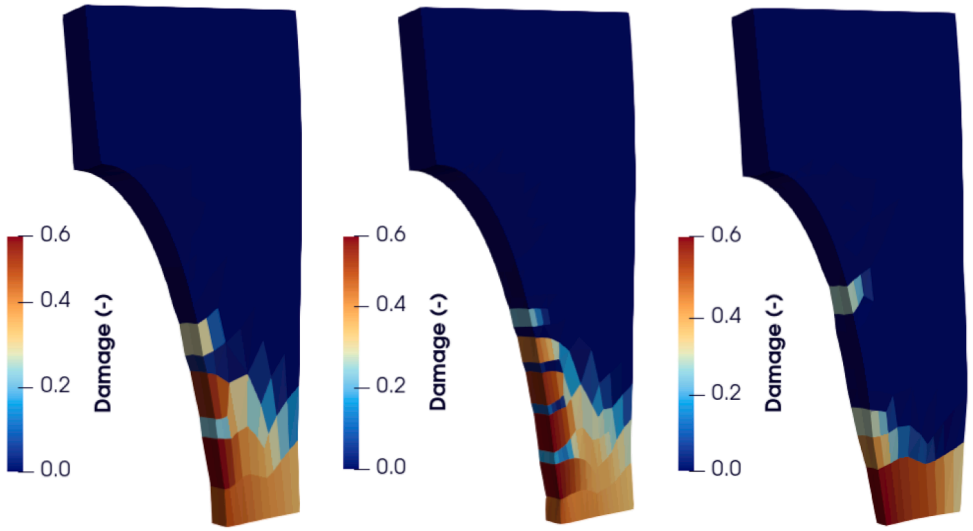

(A) $\boldsymbol{up}$ formulation, Mesh 1 (B) $\boldsymbol{up}$ formulation, Mesh 2 (C) $\boldsymbol{upS'}$ formulation, Mesh 1

Fig. 12. Membrane with a hole. Damage variable D for $\boldsymbol{up}$ and $\boldsymbol{upS'}$ formulations.

mesh refinement, confirming the benefit of interpolating stresses as primary unknowns in problems where the constitutive response and damage evolution are stress-driven.

For the sake of completeness, to quantify the degree to which the mixed formulations satisfy the incompressibility constraint and the constitutive deviatoricity condition associated with the isochoric split, we monitor the norms $\|J-1\|_{L^2}$ and $\|J-1\|_{L^\infty}$, as well as $\|\mathbf{S}' : \mathbf{C}\|_{L^2}$ and $\|\mathbf{S}' : \mathbf{C}\|_{L^\infty}$, along the load steps; see Fig. 13. Here, $\mathbf{S}' : \mathbf{C} = 0$ is the continuum orthogonality condition induced by the deviatoric–volumetric split of the Cauchy stress, while in the present u–p–$\mathbf{S}'$ setting it is recovered through the coupled residual structure and consistent linearization. The results show that both constraints remain well controlled throughout the loading process: the incompressibility defect stays small (with J remaining close to unity) and the deviatoricity defect remains bounded and small relative to the stress level, indicating that the discrete solution recovers $\mathbf{S}' : \mathbf{C} \approx 0$ at convergence for each load increment.

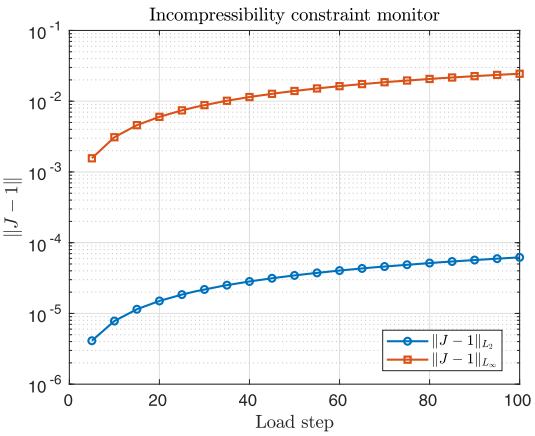

(A) Incompressibility constraint monitor ($\|J-1\|_{L^2}$ and $\|J-1\|_{L^\infty}$).

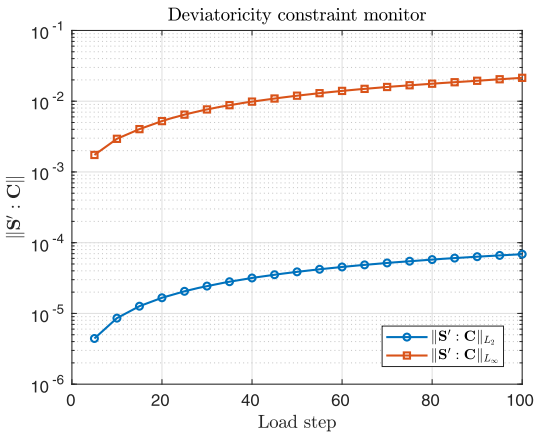

(B) Deviatoricity constraint monitor ($\|\mathbf{S}' : \mathbf{C}\|_{L^2}$ and $\|\mathbf{S}' : \mathbf{C}\|_{L^\infty}$).

Fig. 13. Membrane with a hole. Monitoring of incompressibility and deviatoricity constraints for the mixed formulations.

5. Conclusions

In this work, a stabilized mixed FE formulation involving displacements, pressure, and stresses as primary variables has been presented for finite strain damage models. The approach has been shown to provide several key advantages:

- Improved stress accuracy – By incorporating stresses as unknowns, the formulation delivers significantly more accurate stress fields, which are essential in constitutive models where the material response depends explicitly on stresses. The numerical results demonstrate that the accuracy of the formulation on coarse meshes is comparable to that of displacement–pressure formulations on meshes refined to roughly half the element size. This confirms that introducing stresses as unknowns enables reliable solutions without excessive mesh refinement.
- Robustness in nonlinear regimes – The method performs well in scenarios involving incompressibility, finite strains, and material softening due to damage, maintaining stability and consistency across different benchmark problems.
- Computational competitiveness – Despite introducing additional degrees of freedom, the proposed approach remains competitive, as the reduction in required mesh refinement offsets the increased cost per element.
- Perspectives on localization – The possibility of modeling localization phenomena by computing the damage-driving variable directly in terms of stresses with slight changes in the formulation is a promising avenue that needs to be further explored in finite strain regimes.

Overall, the formulation represents a robust and efficient tool for the accurate simulation of incompressible finite strain damage problems. Its ability to deliver stress-accurate results with coarser discretizations makes it especially attractive for complex nonlinear analyses where mesh-independent stress convergence is critical.

CRediT authorship contribution statement

Inocencio Castañar: Writing – review & editing, Writing – original draft, Validation, Software, Methodology, Investigation, Formal analysis; **Ramon Codina:** Writing – review & editing, Writing – original draft, Supervision, Methodology, Investigation, Funding acquisition, Formal analysis, Conceptualization; **Joan Baiges:** Writing – review & editing, Supervision, Software, Methodology.

Data availability

No data was used for the research described in the article.

Declaration of competing interest

The authors declare that they have no known competing financial interests or personal relationships that could have appeared to influence the work reported in this paper.

Acknowledgement

R. Codina is deeply grateful to Professor Manolis Papadrakakis for his kindness and friendship, and in particular for his personal support and help at a particularly challenging moment, a gesture that will not be forgotten.

R. Codina also gratefully acknowledges the support received through the ICREA Acadèmia Research Program of the Catalan Government.

References

[1] L.M. Kachanov, Rupture time under creep conditions, Int. J. Fract. 97 (1) (1999) 11–18. https://doi.org/10.1023/A:1018671022008
[2] L.M. Kachanov, Introduction to Continuum Damage Mechanics, 10, Springer Netherlands, Dordrecht, 1986. https://doi.org/10.1007/978-94-017-1957-5
[3] J.C. Simo, J.W. Ju, Strain- and stress-based continuum damage models – Parts I and II, Int. J. Solids Struct. 23 (7) (1987) 821–869. https://doi.org/10.1016/0020-7683(87)90083-7
[4] J.W. Ju, On energy-based coupled elastoplastic damage theories: constitutive modeling and computational aspects, Int. J. Solids Struct. 25 (7) (1989) 803–833. https://doi.org/10.1016/0020-7683(89)90015-2
[5] J.L. Chaboche, Continuum damage mechanics: Part I - General concepts, J. Appl. Mech. 55 (1) (1988) 59–64. https://doi.org/10.1115/1.3173661
[6] S. Murakami, Notion of continuum damage mechanics and its application to anisotropic creep damage theory, J. Eng. Mater. Technol. 105 (2) (1983) 99–105. https://doi.org/10.1115/1.3225633
[7] J.W. Ju, Isotropic and anisotropic damage variables in continuum damage mechanics, J. Eng. Mech. 116 (12) (1990) 2764–2770. https://doi.org/10.1061/(ASCE)0733-9399
[8] J.C. Simo, On a fully three-dimensional finite-strain viscoelastic damage model: formulation and computational aspects, Comput. Methods Appl. Mech. Eng. 60 (2) (1987) 153–173. https://doi.org/10.1016/0045-7825(87)90107-1
[9] C. Miehe, Discontinuous and continuous damage evolution in Ogden-type large-strain elastic materials, Eur. J. Mech. A Solids 14 (5) (1995) 697–720.
[10] E.A. de Souza Neto, D. Perić, D.R.J. Owen, Continuum modelling and numerical simulation of material damage at finite strains, Arch. Comput. Methods Eng. 5 (4) (1998) 311–384. https://doi.org/10.1007/BF02905910
[11] J. Diani, B. Fayolle, P. Gilormini, A review on the Mullins effect, Eur. Polym. J. 45 (3) (2009) 601–612. https://doi.org/10.1016/j.eurpolymj.2008.11.017
[12] E. Comellas, F.J. Bellomo, S. Oller, A generalized finite-strain damage model for quasi-incompressible hyperelasticity using hybrid formulation, Int. J. Numer. Methods Eng. 105 (10) (2016) 781–800. https://doi.org/10.1002/nme.5118
[13] I. Castañar, J. Baiges, R. Codina, A stabilized mixed finite element approximation for incompressible finite strain solid dynamics using a total Lagrangian formulation, Comput. Methods Appl. Mech. Eng. 368 (2020) 113164.
[14] R. Codina, I. Castañar, J. Baiges, Finite element approximation of stabilized mixed models in finite strain hyperelasticity involving displacements and stresses and/or pressure—an overview of alternatives, Int. J. Numer. Methods Eng. 125 (18) (2024) e7540. https://doi.org/10.1002/nme.7540
[15] I. Castañar, R. Codina, J. Baiges, A stabilized mixed three-field formulation for stress accurate analysis including the incompressible limit in finite strain solid dynamics, Int. J. Numer. Methods Eng. 124 (10) (2023) 2341–2366.
[16] M. Cervera, M. Chiumenti, R. Codina, Mixed stabilized finite element methods in nonlinear solid mechanics. Part II: strain localization, Comput. Methods Appl. Mech. Eng. 199 (2010) 2571–2589.
[17] M. Cervera, M. Chiumenti, R. Codina, Mixed stabilized finite element methods in nonlinear solid mechanics. Part I: formulation, Comput. Methods Appl. Mech. Eng. 199 (37–40) (2010) 2559–2570.
[18] M. Cervera, M. Chiumenti, R. Codina, Mixed stabilized finite element methods in nonlinear solid mechanics. Part II: strain localization, Comput. Methods Appl. Mech. Eng. 199 (37–40) (2010) 2571–2589.
[19] M. Chiumenti, M. Cervera, R. Codina, A mixed three-field FE formulation for stress accurate analysis including the incompressible limit, Comput. Methods Appl. Mech. Eng. 283 (2015) 1095–1116.
[20] M. Jirásek, Nonlocal damage mechanics, Technical Report, Czech Technical University in Prague, 11 (7–8) (2007) 993–1021. Survey / lecture notes.
[21] L. Sprave, A. Menzel, A large strain gradient-enhanced ductile damage model: finite element formulation, experiment and parameter identification, Acta Mech. 231 (2020) 5159–5192. https://doi.org/10.1007/s00707-020-02786-5
[22] C. Miehe, M. Hofacker, F. Welschinger, Phase-field modeling of ductile fracture at finite strains: a variational gradient-extended plasticity-damage theory, Comput. Mech. 57 (1) (2016) 1–38. https://doi.org/10.1007/s00466-015-1159-4
[23] V. Ambati, R. Kruse, L. De Lorenzis, A phase-field model for ductile fracture at finite strains and its experimental verification, Comput. Mech. 57 (1) (2016) 149–167. https://doi.org/10.1007/s00466-015-1225-4
[24] M.S. Niazi, H.H. Wisselink, T. Meinders, Viscoplastic regularization of local damage models: revisited, Comput. Mech. 51 (2013) 203–216. https://doi.org/10.1007/s00466-012-0722-6
[25] T.J.R. Hughes, Multiscale phenomena: Green's function, the Dirichlet-to-Neumann formulation, subgrid scale models, bubbles and the origins of stabilized formulations, Comput. Methods Appl. Mech. Eng. 127 (1995) 387–401.
[26] T.J.R. Hughes, G.R. Feijóo, L. Mazzei, J. Quincy, The variational multiscale method - a paradigm for computational mechanics, Comput. Methods Appl. Mech. Eng. 166 (1998) 3–24.
[27] R. Codina, Finite element approximation of the three field formulation of the Stokes problem using arbitrary interpolations, SIAM J. Numer. Anal. 47 (2009) 699–718.
[28] J. Riesselmann, J.W. Ketteler, M. Schedensack, D. Balzani, Three-field mixed finite element formulations for gradient elasticity at finite strains, GAMM-Mitteilungen 43 (2020) e202000002. https://doi.org/10.1002/gamm.202000002
[29] J. Riesselmann, D. Balzani, A simple and efficient lagrange multiplier based mixed finite element for gradient damage, Comput. Struct. 281 (2023) 107030. https://www.sciencedirect.com/science/article/pii/S0045794923000603. https://doi.org/10.1016/j.compstruc.2023.107030
[30] D. Balzani, M. Köhler, T. Neumeier, et al., Multidimensional rank-one convexification of incremental damage models at finite strains, Comput. Mech. 73 (2024) 27–47. https://doi.org/10.1007/s00466-023-02354-3
[31] P. Junker, J. Riesselmann, D. Balzani, Efficient and robust numerical treatment of a gradient-enhanced damage model at large deformations, Int. J. Numer. Methods Eng. 123 (3) (2022) 774–793. https://doi.org/10.1002/nme.6876
[32] Z. Ma, X. Feng, W. Hong, Fracture of soft elastic foam, J. Appl. Mech. 83 (2016) 031007.
[33] B. Li, N. Bouklas, A variational phase-field model for brittle fracture in polydisperse elastomer networks, Int. J. Solids Struct. 182 (2020) 193–204.
[34] T. Belytschko, W.K. Liu, B. Moran, Nonlinear Finite Elements for Continua and Structures, Wiley, 2001.
[35] G. Scovazzi, B. Carnes, X. Zeng, S. Rossi, A simple, stable, and accurate linear tetrahedral finite element for transient, nearly, and fully incompressible solid dynamics: a dynamic variational multiscale approach, Int. J. Numer. Methods Eng. 106 (2016) 799–839.
[36] C.O. Horgan, J.G. Murphy, On the volumetric part of strain-energy functions used in the constitutive modeling of slightly compressible solid rubbers, Int. J. Solids Struct. 46 (2009) 3028–3085.
[37] J.C. Simo, J.W. Ju, Strain- and stress-based continuum damage models. I. Formulation, Int. J. Solids Struct. 23 (7) (1987) 821–840. https://doi.org/10.1016/0020-7683(87)90083-7
[38] J.C. Simo, J.W. Ju, Strain- and stress-based continuum damage models. II. Computational aspects, Int. J. Solids Struct. 23 (7) (1987) 841–869. https://doi.org/10.1016/0020-7683(87)90084-9

[39] Y. He, D. Zuo, K. Hackl, H. Yang, S.J. Mousavi, S. Avril, Gradient-enhanced continuum models of healing in damaged soft tissues, Biomech. Model. Mechanobiol. 18 (5) (2019) 1443–1460. https://doi.org/10.1007/s10237-019-01155-z
[40] D. Boffi, F. Brezzi, M. Fortin, Mixed Finite Element Methods and Applications, Springer, 2013.
[41] S. Badia, R. Codina, Unified stabilized finite element formulations for the Stokes and the Darcy problems, SIAM J. Numer. Anal. 47 (3) (2009) 1971–2000.
[42] S. Balay, S. Abhyankar, M.F. Adams, J. Brown, P. Brune, K. Buschelman, L. Dalcin, V. Eijkhout, W.D. Gropp, D. Kaushik, M.G. Knepley, D.A. May, L.C. McInnes, R.T. Mills, T. Munson, K. Rupp, P. Sanan, B.F. Smith, S. Zampini, H. Zhang, H. Zhang, PETSc Web page, 2015, (http://www.mcs.anl.gov/petsc).
[43] I. Castañar, J. Martínez-Frutos, R. Ortigosa, R. Codina, Stabilized mixed formulations for incompressible finite strain electromechanics including stress accurate analysis, Int. J. Numer. Methods Eng. 126 (22) (2025) e70089. https://doi.org/10.1002/nme.70089